NC 4'11483

NASA TN D-909

IN-08
2862-598

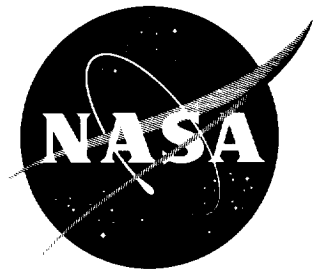

TECHNICAL NOTE

D-909

ANALYTICAL INVESTIGATION OF AN ADAPTIVE FLIGHT-CONTROL SYSTEM USING A SINUSOIDAL TEST SIGNAL

By Jack E. Harris

Langley Research Center
Langley Field, Va.

NATIONAL AERONAUTICS AND SPACE ADMINISTRATION
WASHINGTON June 1961

1K

NATIONAL AERONAUTICS AND SPACE ADMINISTRATION

TECHNICAL NOTE D-909

ANALYTICAL INVESTIGATION OF AN ADAPTIVE FLIGHT-CONTROL SYSTEM USING A SINUSOIDAL TEST SIGNAL

By Jack E. Harris

L
1
4
5
5

SUMMARY

An analytical study was made of an adaptive flight-control system which measures vehicle response to small-amplitude control-surface deflections produced by a sinusoidal test signal. Changes in the response to this signal are related to environmental changes, and the system is continuously altered to maintain this response equal to a preselected value. The system is suitable for use in high-performance aircraft and missiles and requires only the addition of a signal generator and a logic circuit consisting of a filter-rectifier network and a comparator-integrator network to a basic command-control system. Thus, it presents a relatively simple approach to the problem.

The effects on system performance of variation in flight condition, system-gain level, test-signal frequency, and sensor location are included in the analysis. Longitudinal control of a high-performance research aircraft over flight conditions ranging from landing approach to a Mach number of 5.8 at an altitude of 150,000 feet, and longitudinal control of a four-stage solid-fuel missile including the first bending mode over the atmospheric portion of a launch trajectory constituted the basis for the analytical study.

Results of an analog-computer study using time-varying coefficients are presented to compare the control obtained with the adaptive system with that obtained with a fixed-gain system during the atmospheric portion of a missile launch trajectory.

The system has demonstrated an ability to maintain satisfactory vehicle control-system stability over wide ranges of environmental change.

INTRODUCTION

The control problem associated with present-day aircraft and missiles has been greatly increased by the operational requirements of these vehicles. The wide ranges of Mach number and altitude, coupled with wide changes in center-of-gravity position (sometimes nearing 20 percent of the vehicle length during the atmospheric portion of a missile trajectory), cause the stability and control characteristics to vary greatly. Often these characteristics vary so much that they are unsatisfactory during portions of the desired flight envelope.

L
1
4
5
6

Automatic-control systems and stability-augmentation devices have been installed in most high-performance vehicles to provide satisfactory stability and control characteristics. Automatic longitudinal flight-control systems in present use require variations of control-system parameters. These parameters are varied as programed functions of the flight conditions, such as airspeed, altitude, or time. For adequate programs, knowledge of the stability and control characteristics throughout the flight envelope is required. This knowledge in turn requires wind-tunnel tests, backed up by lengthy flight-test programs.

A system capable of measuring its response, comparing this measured response with a desired standard, and modifying its parameters in a closed-loop fashion to obtain the desired response might greatly reduce the required flight-test program and produce a more closely integrated control system. Such a system is called an adaptive control system.

The potentialities of adaptive controls in handling the increased problems of control of aircraft have produced a great deal of interest. Most adaptive concepts can be summarized as follows:

(1) Those that use the system response to a normal input, such as a pilot input or external disturbance, to modify the system parameters.

(2) Those that use the system response to an internal continuous test signal to modify the system parameters.

(3) Those that use some specific system interrelationship, such as control gain associated with neutral stability of one of the system components, to adjust the system parameters.

Specific examples of each type can be found in reference (1).

An automatic longitudinal-flight-control system that affords the pilot a constant ratio of pitch rate per pilot input command has been shown to be desirable (ref. 2). This ratio is easily obtained by a feedback control system with an integration in the forward loop. However,

it is necessary now to be concerned with the stability of the system, which can change due to changes in the controlled element.

With the integration, the open-loop gain for a zero frequency excitation is infinite regardless of the variation in the controlled element; however, the system gain at a frequency other than zero is not infinite and is altered by the changes in the characteristics in the controlled system. One such characteristic is control effectiveness which varies with Mach number and dynamic pressure. This principle suggested the use of a system of the second type; that of measuring the vehicle response to a high-frequency, small-amplitude, sinusoidal test signal producing oscillatory control-surface deflections. The control gain is automatically varied to maintain the output pitch rate due to the test signal equal to a preselected constant. A narrow-band-pass filter is used to separate the response to the test signal from the response to other inputs. The purpose of this paper is to investigate the principle of operation; namely, to determine if adequate aircraft stability can be maintained by automatically varying the control gain level so that the controlled system response (as measured by vehicle pitch-rate response to a sinusoidal test signal) is kept constant.

Included in this paper are the effects on system performance of variations in flight condition, system gain level, test-signal frequency, and sensor location. Results of an analog-computer study using a time-varying-coefficient program for a flexible missile are presented to compare the control obtained with the adaptive system with that obtained with a fixed-gain system, and to determine the transient characteristics of the adaptive loop and the effect of these characteristics on the over-all stability of the flight-control system.

SYMBOLS

$A(s)$ transfer function of airframe pitching velocity to control deflection

a_i area of ith section, sq in.

$C_{L,i}$ lift coefficient of ith section, $\frac{L_i}{qa_i}$

d_i normalized displacement of first bending mode at the force station of the ith section, in./in.

e	error signal in adaptive loop
F(s)	filter transfer function
F_Z	force along Z-axis, lb
H(s)	hydraulic actuator transfer function
h	displacement of reference point to which the first bending mode is normalized, in.
I(s)	adaptive-loop error shaping network transfer function
I_Y	moment of inertia about the Y-axis, lb-in./sec^2
$j\omega$	imaginary portion of the complex variable $s = \sigma \pm j\omega$, radians/sec
K_v	amplifier gain, dimensionless
L_i	lift force of the ith section, positive upward, lb
l_i	length between the missile center of gravity and the assumed force station of the ith section, in.
M_Y	pitching moment about the Y-axis, in-lb
m	mass, lb-sec^2/in.
m_b	generalized mass of the first bending mode, lb-sec^2/in.
N(s)	forward-loop shaping network transfer function
Q_b	generalized force input to the first bending mode, lb
q	dynamic pressure of air stream, lb/sq in.
q_e	dynamic pressure of exhaust stream, lb/sq in.
R(s)	rectifier transfer function
s	Laplace operator, per sec
u	linear velocity component along the X-axis, in./sec
V_o	linear velocity along flight path, in./sec

L 1 4 5 6

w	linear velocity component along the Z-axis, in./sec
α	angle of attack, radians
α_i	local angle of attack of ith section measured at the assumed force station, radians
δ	control-surface deflection (tip control plus jet vane), radians
ϵ	forward-loop error signal
ζ	damping ratio of linear second-order system particularized by the subscript
θ	angular displacement about the Y-axis, radians
λ_i	slope of normalized first bending mode at the force station of the ith section, per in.
λ_j	slope of normalized first bending mode at station j, per in.
σ	real portion of the complex variable $s = \sigma \pm j\omega$, sec^{-1}
τ_a	aircraft path time constant, sec
ϕ	angular displacement about the X-axis, radians
ψ	angular displacement about the Z-axis, radians
ω	undamped natural frequency of second-order mode particularized by the subscript, radians/sec

Subscripts:

b	first bending mode
c	input command
G	output measured at the center of gravity
g	output measured at sensor location
r	rectified version of signal
s	airframe short period
t	test signal

pitching-velocity signal to the input test-signal amplitude as a function of test-signal frequency are shown in figure 3 for the three flight

6

1 2 3 4 sections along missile body

8

conditions of figure 2. This ratio $\dot{\theta}_g/\dot{\theta}_t$ will be referred to as closed-loop dynamic gain. The frequency and damping-ratio characteristics of the system components used in the calculation of figure 3 represent those associated with the maximum and minimum control gains for that particular flight condition as determined by the root-locus study. Each value of closed-loop dynamic gain included between the boundary curves corresponds to a value of steady-state control gain associated with satisfactory short-period characteristics for that flight condition.

Figure 4 is a superposition of the plots of figure 3. The shaded area starting at a frequency of about 8 radians/sec represents combinations of test-signal frequency and closed-loop dynamic gain common to all the flight conditions. Thus, while there is no value of steady-state control gain common to the flight conditions investigated, there are certain test-signal-frequency ranges where there are values of closed-loop dynamic gain common to each, and each combination of frequency and gain represents a satisfactory steady-state control gain level. One such value of closed-loop dynamic gain at a particular frequency is used as a basis for the bias value and for the frequency of the test signal. Thus, as the control effectiveness varies, due to environmental change the control gain can be forced automatically to vary in such a manner as to maintain the closed-loop dynamic gain constant and in so doing will produce satisfactory short-period characteristics.

L 1 4 5 6

Application to Missile Control

The investigation was extended to include control of a flexible missile in order to further evaluate the system's ability to compensate for rapid changes in control effectiveness and to include the effects of flexibility and sensor location. A four-stage, solid-fuel launch vehicle with a longitudinal pitch-rate control system incorporating tip control flaps located on horizontal stabilizing fins and jet vanes immersed in the exhaust stream was chosen for the study. The resultant control effectiveness decreases rapidly after first-stage burnout due to the loss in effectivensss of the exhaust-stream vanes. A transfer function relating missile pitching-velocity response to control-surface deflection was obtained by the method described in appendix A. Numerical values of the coefficients of the variables in the equations of motion were calculated as a function of trajectory flight time by a digital-computer program from unpublished vibration and static-stability data for the test missile.

The transfer-function values used in obtaining the system closed-loop equation are listed in table 3. The control system used in this portion of the study is still that shown in figure 1.

Root-locus plots showing the variations in the short-period and first-bending-mode characteristics as a function of control gain are shown in figure 5. Figures 5(a), 5(b), and 5(c) represent three time periods along the trajectory for the same missile characteristics; whereas figure 5(d) is for a case with a higher frequency first bending mode, and 5(e) is for a case with a different sensor location. The sensor station numbers represent the number of inches between the sensor location and a reference point, which for the missile used, was the first-stage nozzle exit. Station 400 represents a location in the transition section between the first and second stages, and station 646 represents a location in the section between the second and third stages. The first-bending-mode slope value λ_j at station 400 was 0.000 and was 0.0037 per inch at station 646.

L
1
4
5
6

Since missiles generally operate with lower damping than aircraft, the limits of satisfactory short-period characteristics were extended from those associated with the aircraft to include damping ratios of 0.2. The satisfactory region is shown in figure 5. A further condition imposed, was that the damping ratio of the bending mode should not be lowered below the missile's basic value of 0.01 in attaining increased short-period damping, since the damping was initially low.

The maximum and minimum values of steady-state control gain for the conditions shown in figure 5 are presented in table 4. No value of control gain is common to these flight conditions. It is of note, however, that a 34-percent change in first-mode bending frequency did not significantly alter the satisfactory control gain range although the value of control gain associated with neutral stability was changed. Also, a change in station location which represented a substantial change in the value of the bending-mode slope did not change the range of satisfactory values of control gain from those of the initial sensor location.

This indicates that a margin of error in the knowledge of bending frequency and mode shape may be tolerable with this type of control; however, the magnitude of this error margin was not investigated further than the conditions shown.

The closed-loop frequency response plots of the ratio of the measured missile pitching-velocity-signal amplitude to the test-signal amplitude as a function of the test-signal frequency are shown in figure 6 for three flight conditions with the same missile configuration. The frequency and damping ratio characteristics of the system components used in the calculations were determined in the same manner as in the analysis of the longitudinal control of the high-performance research aircraft. Figure 7 is a superposition of figures 6(a), 6(b), and 6(c).

The shaded region represents combinations of test-signal frequencies and closed-loop dynamic gains common to the various flight conditions.

Thus, for example, if the adaptive loop would maintain the ratio of the output-to-input amplitude of a 15 radians/sec test signal equal to -5 db, the missile short-period characteristics would be kept satisfactory, and the first bending mode would have increased damping throughout the atmospheric flight envelope. This -5 db value of dynamic gain assumes unity gain of the filter and rectifier, and if these gains were not unity, the bias value would have to be altered to account for the additional amount of gain present.

ANALOG COMPUTER SIMULATION

Description of Adaptive Loop

The previous analysis methods were based on the assumption of linear system characteristics; however, any actual control system will exhibit some nonlinear characteristics due to such things as velocity limiting of the control actuator and position limiting of the control surfaces. An analog-computer simulation (see appendix B) of the missile-plus-control system analytically studied was conducted to indicate a more realistic estimate of the control available with the adaptive system, and to determine the transient characteristics of the adaptive loop. The transfer characteristics of the forward-loop shaping network $N(s)$ and adaptive-loop filter $F(s)$ and rectifier $R(s)$ were realized by the use of d.c. amplifiers with suitable input and feedback networks. Three adaptive-loop band-pass filters of different values of selectivity were tested. The output-to-input relationship of the filters in Laplace notation is as follows:

$$\dot{\theta}_t'/\dot{\theta}_g = \frac{Ks}{1 + 2\zeta/\omega s + 1/\omega^2 s^2} \qquad (1)$$

Suitable values of resistance and capacitance were chosen so that functions equivalent to damping ratios of 0.1, 0.05, and 0.005, with natural frequencies of 15 radians/sec, could be simulated. The gain K was unity. In all further references the numbers 0.1, and so forth, on the filters refer to their equivalent damping ratio. The filter characteristics were such that filter 0.05, while being more selective, had a slower transient response time by a factor of approximately 5, as compared with filter 0.1. Filter 0.005 had such a slow response that it was unsatisfactory.

Ideally, the adaptive-loop shaping network $I(s)$ should be an integrator with a very high gain so that the amplifier gain K_v will be quickly adjusted to a value that will null the error signal e; however, it was found necessary to add a signal proportional to the error itself to provide damping for the amplifier gain K_v. The gains of the two signals, e and $\int e dt$, were adjusted to produce as rapid a change in amplifier gain per change in error signal e as possible and still not have excessive overshoot of the amplifier gain. These values were maintained throughout the remainder of the program. The resulting network transfer function is given by the following equation:

L
1
4
5
6

$$e'/e = 0.5(1/s + 0.6) \tag{2}$$

The trajectory characteristics used in this study are shown in figure 8 and represent the portion of the flight between launch and second-stage ignition.

Results of Computer Study

Missile-trajectory time histories showing the response to a sharp-edge gust disturbance are shown in figure 9. All cases represent control by the adaptive system with a sensor located at station 646; however, figures 9(d), 9(e), and 9(f) represent runs having increased sensitivity in the gain changing loop. Proper operation of the control system should cause the vehicle pitch rate to return to a value of zero following a disturbance.

The disturbance was introduced into the simulation as a 1° step change in angle of attack; however, the notation on the figure is that of the more familiar horizontal wind velocity in ft/sec. This change in angle is related to horizontal wind velocity by the relationship

$$\Delta\alpha_w = \tan^{-1} \frac{U_n}{V_v} \tag{3}$$

where V_v is the missile vertical velocity component represented by the velocity along the flight path since the missile path is nearly vertical, U_n is the horizontal wind velocity component, and $\Delta\alpha_w$ is the change in angle of attack due to the wind. The 1° change is equivalent to wind velocities somewhat larger than the missile might be expected to encounter.

Proper operation of the adaptive loop should maintain the rectified test signal $\dot{\theta}'_{t,r}$ equal to the bias; however, this signal decreases somewhat during the later portion of the trajectory indicating a lag is

present in the adaptive loop. This lag is apparently caused by a limitation in the maximum rate of change of error signal e, allowing a lag in the change of the amplifier gain K_v. However, the gain is increased sufficiently in order to damp adequately any pitching oscillation produced by the disturbance, as shown by the $\dot{\theta}_g$ trace.

In order to try to increase the maximum rate of change of e, both the bias and the rectified test signals were increased by a factor of 3 in the simulation; thus the same reference ratio was maintained but the amplitude of the error signal e for a given change in the rectified test signal was increased. As shown in figures 9(d), 9(e), and 9(f), this increase in maximum rate resulted in a more rapid increase in control gain but also appeared to cause an overshoot in the control gain, and secondary oscillations are evident in pitching velocity and bending traces. Thus, this increase resulted in the same conditions as previously mentioned in the discussion of the mechanization of I(s). The control gain was limited to a value of 80 in order to restrict the maximum amplitude of the control-surface oscillations to plus or minus 5° during the latter portions of the trajectory.

The effect of filter characteristics can best be illustrated by a comparison of figures 9(b) and 9(h). The harmonic content of the disturbance signal was sufficient to cause an apparent increase in the test-signal amplitude as shown by the increase in $\dot{\theta}'_{t,r}$ after 30 seconds of flight time had elapsed. This apparent increase was more pronounced in the 0.1 filter due to its wider bandwidth. This apparent increase in excitation signal amplitude caused the adaptive loop to lower the control gain. This decreased value was less than the minimum value for satisfactory stabilization, and following the disturbance increased amounts of pitch-rate and bending oscillations may be noticed. This apparent increase in test-signal amplitude appeared to be a function of both the selectivity and time constant of the filter. Some trade-off in the two is necessary in obtaining the best filter characteristics. Of the two shown, the 0.05 filter held the rectified signal $\dot{\theta}'_{t,r}$ more nearly constant in the presence of extraneous signals and was felt to be a satisfactory compromise.

Missile time histories showing vehicle response to a sharp-edge gust disturbance when controlled by a fixed-gain system are shown in figure 10. The fixed-gain type of system represents the type presently incorporated in the missile. A control-gain value of 5 was used since it represented the value presently used in the test missile. The sensor was located at station 646.

The maximum amplitude of the pitch-rate and bending oscillations caused by the disturbance are similar for control by either system, but the time required to damp out the pitch-rate oscillations varies both

with type of system and system components. The damping times for the various systems and combinations of components are compared in table 5. An evident advantage of the adaptive system is its ability to damp the pitch-rate oscillations in the latter portions of the trajectory. This increased damping will decrease the attitude errors present at the second-stage ignition.

Another feature of the system is an ability to prevent instability induced by control sensitivity. The test-signal frequency needs to be near the frequency associated with neutral stability of some mode. As an increased value of forward-loop gain increases the tendency of the mode to become unstable, the dynamic gain should increase sharply. This increase should, in turn, call for a lower control gain through the adaptive loop. The operation of this feature was examined with the aid of the analog mechanization. The forward-loop gain is comprised of the network gain, amplifier gain, and actuator gain. A circuit was incorporated in the mechanization to alter the network gain, which previously had been unity, without changing the amplifier and actuator gains. The network gain was given a step increase calculated to produce a value of forward-loop gain associated with instability, such as might be encountered due to some partial electronic failure or apparent decrease in control effectiveness due to test-signal drift which would call for increased control gain through the adaptive loop. The results of this increase are shown in figure 11. Immediately following the network gain increase, initiated after 30 seconds of flight time, the vehicle became unstable (flat tops of the peaks represent the physical limitations of the recorder, not the response quantity itself); however, the amplifier gain (represented on the figure as control gain) decreased to its minimum value, and control was restored. Later, the rectifier signal $\dot{\theta}'_{t,r}$ was less than the bias and called for an increase in control gain. Since the amplifier gain was being multiplied by a large network gain, the forward-loop gain was very sensitive to amplifier gain changes, and after 41 seconds had elapsed, divergence started again but was quickly checked by a decrease in the amplifier gain. Network gain increases were initiated at several other points during the trajectories and the flight of figure 11 represents the most serious case; that is, the one that took the longest time to restore control. A similar run made with a fixed-gain system resulted in complete loss of control.

The effect of sensor location on the adaptive control system's performance is shown in figure 12. However, all the locations investigated had positive bending-mode slopes. It is evident that the bending slope at the sensor location has an appreciable effect on the magnitude of the bending induced by the test signal. The larger the bending slope at the sensor location the greater the induced bending. The maximum amplitude of the excursions caused by the gust, and the time required to damp out these excursions, are similar, although the bias used in

all cases was based on a response ratio with a sensor location at station 646. This similarity agrees with the results of the root-locus study which showed that the range of satisfactory control-gain values was similar for the different locations although the values associated with neutral stability were quite varied.

CONCLUDING REMARKS

The results of the investigation indicated that it is possible to maintain satisfactory longitudinal short-period characteristics over a wide range of flight conditions, ranging from landing approach at a Mach number of 0.5 to a Mach number of 5.8 at an altitude of 150,000 feet for a high-performance research aircraft and over the atmospheric portion of a missile trajectory, by varying the steady-state control gain so that the closed-loop dynamic gain is kept constant. The dynamic gain is defined as the ratio of the vehicle pitch-rate response to a sinusoidal test signal at a particular frequency. Maintaining stability was possible despite the fact that common values of steady-state control gain associated with satisfactory longitudinal short-period characteristics did not exist for the wide ranges of flight conditions investigated because there were test-signal-frequency ranges where there were values of closed-loop dynamic gain common to each condition, and each value of dynamic gain represented a satisfactory value of steady-state control gain.

The adaptive loop entailed only the addition to a rate-command control system of a logic circuit comprised of a filter-rectifier network and a comparator-integrator network and was simple in concept; however, some prior knowledge of the characteristics of a particular vehicle would be needed to determine the test-signal-frequency range and bias values that can be used for that vehicle.

Also, care must be taken in locating the feedback sensor since the greater the value of the bending slope at the sensor location, the greater the induced bending.

The sensitivity and selectivity of the filter somewhat limited the effectiveness of the system, but a suitable compromise was obtained and the adaptive system proved itself capable of closer path control of a missile during periods of low control effectiveness than fixed-gain systems yet did not overcontrol during periods of high control effectiveness.

In addition, the system demonstrated an ability to prevent instability induced by increased control sensitivity due to some system malfunction.

Langley Research Center,
National Aeronautics and Space Administration,
Langley Field, Va., April 20, 1961.

L
1
4
5
5

APPENDIX A

DEVELOPMENT OF MISSILE PERTURBATION EQUATIONS OF MOTION

The axis system employed and positive direction of forces, moments, and displacements are shown in figure 13.

The small perturbation equations for the rigid body longitudinal case can be written as follows (ref. 4):

$$F_Z = m\left(\dot{w} - V_o\dot{\theta}_G\right) \tag{A1}$$

$$M_Y = I_Y\ddot{\theta}_G \tag{A2}$$

The elastic equation for the first mode is (ref. 4)

$$Q_b = m_b\left(\ddot{h} + 2\zeta_b\omega_b\dot{h} + \omega_b{}^2h\right) \tag{A3}$$

The force along the Z-axis is approximately equal in magnitude to the summation of the lift produced by the various sections of the missile and opposite in direction within the region of small angles of attack.

The lift produced by each section can be expressed by:

$$L_i = qa_i\left(C_{L_\alpha}\right)_i\alpha_i \tag{A4}$$

The aerodynamic force inputs were assumed to act at four force stations along the missile body plus at the centers of pressure of the horizontal fins, horizontal tip control surfaces, and the jet vanes. Substituting equation (A4) into equation (A1) yields

$$-m\left(\dot{w} - V_o\dot{\theta}_G\right) = \sum_{i=1}^{5} qa_i\left(C_{L_\alpha}\right)_i\alpha_i + \left[qa_6\left(C_{L_\delta}\right)_6 + q_ea_7\left(C_{L_\delta}\right)_7\right]\delta \tag{A5}$$

The total pitching moment is equal to the summation of the products of the individual applied forces and their lever arms; therefore, equation (A2) becomes:

$$I_Y\ddot{\theta}_G = \sum_{i=1}^{5} qa_i\left(C_{L_\alpha}\right)_i \alpha_i l_i + \left[qa_6\left(C_{L_\delta}\right)_6 l_6 + q_e a_7\left(C_{L_\delta}\right)_7 l_7\right]\delta \qquad (A6)$$

The generalized force associated with the first mode is composed of the summation of the amounts of work done by the individual forces in producing their relative displacements d_i. Therefore, equation (A3) becomes:

$$m_b\left(\ddot{h} + 2\zeta_b\omega_b\dot{h} + \omega_b{}^2 h\right) = \sum_{i=1}^{5} qa_i\left(C_{L_\alpha}\right)_i \alpha_i d_i + \left[qa_6\left(C_{L_\delta}\right)_6 d_6 + q_e a_7\left(C_{L_\delta}\right)_7 d_7\right]\delta \qquad (A7)$$

The local angle of attack can be expressed in the following manner (ref. 4):

$$\alpha_i = \frac{w}{V_o} - \frac{l_i}{V_o}\dot{\theta}_G - \frac{d_i\dot{h}}{V_o} - \lambda_i h \qquad (A8)$$

further

$$\frac{w}{V_o} = \alpha \qquad (A9)$$

By applying equations (A8) and (A9) to equations (A5), (A6), and (A7), the following equations may be obtained:

$$\dot{\alpha} = -\left[\frac{q}{mV_o}\sum_{i=1}^{5} a_i\left(C_{L_\alpha}\right)_i\right]\alpha + \left[1 + \frac{q}{mV_o{}^2}\sum_{i=1}^{5} a_i\left(C_{L_\alpha}\right)_i l_i\right]\dot{\theta}_G + \left[\frac{q}{mV_o{}^2}\sum_{i=1}^{5} a_i\left(C_{L_\alpha}\right)_i d_i\right]\dot{h} + \left[\frac{q}{mV_o}\sum_{i=1}^{5} a_i\left(C_{L_\alpha}\right)_i \lambda_i\right] h - \left\{\frac{1}{mV_o}\left[qa_6\left(C_{L_\delta}\right)_6 + q_e a_7\left(C_{L_\delta}\right)_7\right]\right\}\delta \qquad (A10)$$

$$\ddot{\theta}_G = -\left[\frac{q}{I_Y V_o}\sum_{i=1}^{5} a_i\left(C_{L_\alpha}\right)_i l_i^2\right]\dot{\theta}_G + \left[\frac{q}{I_Y}\sum_{i=1}^{5} a_i\left(C_{L_\alpha}\right)_i l_i\right]\alpha$$

$$-\left[\frac{q}{I_Y V_o}\sum_{i=1}^{5} a_i\left(C_{L_\alpha}\right)_i l_i d_i\right]\dot{h} - \left[\frac{q}{I_Y}\sum_{i=1}^{5} a_i\left(C_{L_\alpha}\right)_i l_i \lambda_i\right]h$$

$$+\left\{\frac{1}{I_Y}\left[q a_6\left(C_{L_\delta}\right)_6 l_6 + q_e a_7\left(C_{L_\delta}\right)_7 l_7\right]\right\}\delta \qquad \text{(A11)}$$

$$\ddot{h} = -\left\{2\zeta_b\omega_b + \left[\frac{q}{m_b V_o}\sum_{i=1}^{5} a_i\left(C_{L_\alpha}\right)_i d_i^2\right]\right\}\dot{h} - \left\{\omega_b^2 + \frac{q}{m_b}\left[\sum_{i=1}^{5} a_i\left(C_{L_\alpha}\right)_i d_i \lambda_i\right]\right\}h$$

$$+\left[\frac{q}{m_b}\sum_{i=1}^{5} a_i\left(C_{L_\alpha}\right)_i d_i\right]\alpha - \left[\frac{q}{m_b V_o}\sum_{i=1}^{5} a_i\left(C_{L_\alpha}\right)_i d_i l_i\right]\dot{\theta}_G$$

$$+\left\{\frac{1}{m_b}\left[q a_6\left(C_{L_\delta}\right)_6 d_6 + q_e a_7\left(C_{L_\delta}\right)_7 d_7\right]\right\}\delta \qquad \text{(A12)}$$

Usually the equations will be solved numerically rather than in symbolic form with the various parameters combined to form a numerical coefficient for each variable. In order to aid in outlining the procedure for solving these equations the coefficients will be represented by K_n (n varies from 1 to 15). Equations (A10), (A11), and (A12) may now be written as

$$\ddot{\alpha} = K_1\alpha + K_2\dot{\theta}_G + K_3\dot{h} + K_4 h + K_5\delta \qquad \text{(A13)}$$

$$\ddot{\theta}_G = K_6\alpha + K_7\dot{\theta}_G + K_8\dot{h} + K_9 h + K_{10}\delta \qquad \text{(A14)}$$

$$\ddot{h} = K_{11}\alpha + K_{12}\dot{\theta}_G + K_{13}\dot{h} + K_{14}h + K_{15}\delta \qquad \text{(A15)}$$

L 1456

Equations (A13), (A14), and (A15) may be written in Laplace transform notation

$$\left(s - K_1\right)\alpha(s) - K_2\theta_G(s) - \left(K_3 s + K_4\right)h(s) = K_5\delta(s) \tag{A16}$$

$$\left(s - K_7\right)\dot{\theta}_G(s) - K_6\alpha(s) - \left(K_8 s + K_9\right)h(s) = K_{10}\delta(s) \tag{A17}$$

$$\left(s^2 - K_{13}s - K_{14}\right)h(s) - K_{11}\alpha(s) - K_{12}\dot{\theta}_G(s) = K_{15}\delta(s) \tag{A18}$$

L
1
4
5
6

The desired relationship is the transform of missile pitching velocity as measured by a sensor per control-surface deflection $\dot{\theta}_g(s)/\delta(s)$. The sensing element is located at some station j on the body; thus the pitching velocity at this station is (from ref. 4)

$$\dot{\theta}_g = \dot{\theta}_G + \lambda_j\dot{h} \tag{A19}$$

The $\dot{\theta}_g(s)/\delta(s)$ relationship may be obtained from the following relationship.

$$\dot{\theta}_G(s)/\delta(s) + \lambda_j\dot{h}(s)/\delta(s) = \dot{\theta}_g(s)/\delta(s) \tag{A20}$$

Equations (A16), (A17), and (A18) may easily be solved by the method of determinants to obtain the desired relationships of equation (A20).

APPENDIX B

Detailed wiring diagrams of the analog mechanization of the aerodynamic equations and control-system simulation are shown in figures 14, 15, and 16. In these figures, r indicates resistance measured in ohms; c, capacitance measured in μf; and τ_h, hydraulic actuator time constant, measured in seconds. Initial conditions are indicated by IC.

L
1
4
5
6

REFERENCES

1. Gregory, P. C., ed.: Proceedings of the Self Adaptive Flight Control Systems Symposium. WADC Tech. Rep. 59-49, ASTIA Doc. No. AD 209389, U.S. Air Force, Mar. 1959.

2. Russell, Walter R., Sjoberg, S. A. and Alford, William L.: A Flight Investigation of the Handling Characteristics of a Fighter Airplane Controlled Through a Rate Type of Automatic Control System. NACA RM L56F06, 1956.

3. Evans, Walter R.: Control-System Dynamics. McGraw-Hill Book Co., Inc., 1954.

4. J. B. Rea Co., Inc.: Aeroelasticity in Stability and Control. WADC Tech Rep. 55-173, U.S. Air Force, Mar. 1957.

L
1
4
5
6

TABLE 1.- CONTROL-SYSTEM TRANSFER FUNCTIONS FOR A HIGH-PERFORMANCE RESEARCH AIRPLANE

$$\left[N(s) = \frac{0.5s + 1}{s(0.05s + 1)};\ H(s) = \frac{1}{(0.04s + 1)}\right]$$

Flight condition		A(s)
Mach number	Altitude, ft	
0.5	20,000	$\frac{1.875(1.31s + 1)}{0.349s^2 + 0.45s + 1}$
5.5	70,000	$\frac{0.252(3.91s + 1)}{0.0605s^2 + 0.0296s + 1}$
5.8	150,000	$\frac{0.006(106.5s + 1)}{0.628s^2 + 0.0119s + 1}$

L 1 4 5 6

L
1
4
5
6

TABLE 2.- MAXIMUM AND MINIMUM VALUES OF CONTROL GAIN OF A HIGH-PERFORMANCE RESEARCH AIRCRAFT

Flight condition		Maximum gain	Minimum gain
Mach number	Altitude, ft		
0.5	20,000	1.3	0.2
5.5	70,000	0.6	0.4
5.8	150,000	10.0	4.0

TABLE 3.- CONTROL-SYSTEM TRANSFER FUNCTIONS OF A FLEXIBLE MISSILE

$$\left[N(s) = \frac{0.5s + 1}{s(0.034s + 1)(0.045s + 1)}; \; H(s) = \frac{1}{0.04s + 1}\right]$$

Flight condition		Sensor station	ω_b, radians/sec	A(s)
Mach number	Altitude, ft			
1	5,000	646	22.4	$\frac{0.0073(17.7s + 1)(0.055s + 1)(-0.054s + 1)}{(0.1475s^2 + 0.0604s + 1)(0.00199s^2 + 0.001435s + 1)}$
3.25	35,000	646	22.4	$\frac{0.0374(10.7s + 1)(0.039s + 1)(-0.038s + 1)}{(0.28s^2 + 0.084s + 1)(0.00199s^2 + 0.00131s + 1)}$
3.6	100,000	646	22.4	$\frac{0.00055(230s + 1)(0.027s + 1)(-0.025s + 1)}{(3.08s^2 + 0.0554s + 1)(0.00199s^2 + 0.0089s + 1)}$
3.25	35,000	646	30.0	$\frac{0.0467(9.1s + 1)(0.028s + 1)(-0.0276s + 1)}{(0.28s^2 + 0.084s + 1)(0.0011s^2 + 0.00102s + 1)}$
3.6	100,000	400	22.4	$\frac{0.00037(348s + 1)(0.00199s^2 + 0.00091s + 1)}{(3.08s^2 + 0.055s + 1)(0.00199s^2 + 0.00090s + 1)}$

L
1
4
5
6

TABLE 4.- MAXIMUM AND MINIMUM VALUES OF CONTROL GAIN OF A FLEXIBLE MISSILE

Flight condition		Sensor station	ω_b, radians/sec	Control gain	
Mach number	Altitude, ft			Maximum	Minimum
1	5,000	646	22.4	11.0	4.0
3.25	35,000	646	22.4	7.0	2.0
3.6	100,000	646	22.4	200.0	60.0
3.25	35,000	646	30.0	6.0	2.0
3.6	100,000	400	22.4	200.0	60.0

TABLE 5.- DAMPING TIMES FOR SEVERAL COMBINATIONS OF CONTROL-SYSTEM COMPONENTS

Point in trajectory where disturbance is encountered in flight, sec	Time required to damp $\dot{\theta}$ to zero, sec			
	Adaptive system with filter 0.05	Adaptive system with filter 0.05 and increased error sensitivity	Adaptive system with filter 0.1	Fixed-gain system
10	2.0	4.0	4.0	4.0
15	1.0	.8	1.2	3.0
20	.6	8.0	5.0	2.0
25	.5	10.0	7.2	2.0
30	.4	10.0	7.0	1.0
35	1.2	4.0	13.0	1.2
40	1.0	.8	10.0	8.0
45	6.5	4.0	7.0	24.0
50	7.5	4.0	6.0	Undamped
55	6.0	2.5	6.0	Undamped
60	3.4	1.5	3.0	Undamped

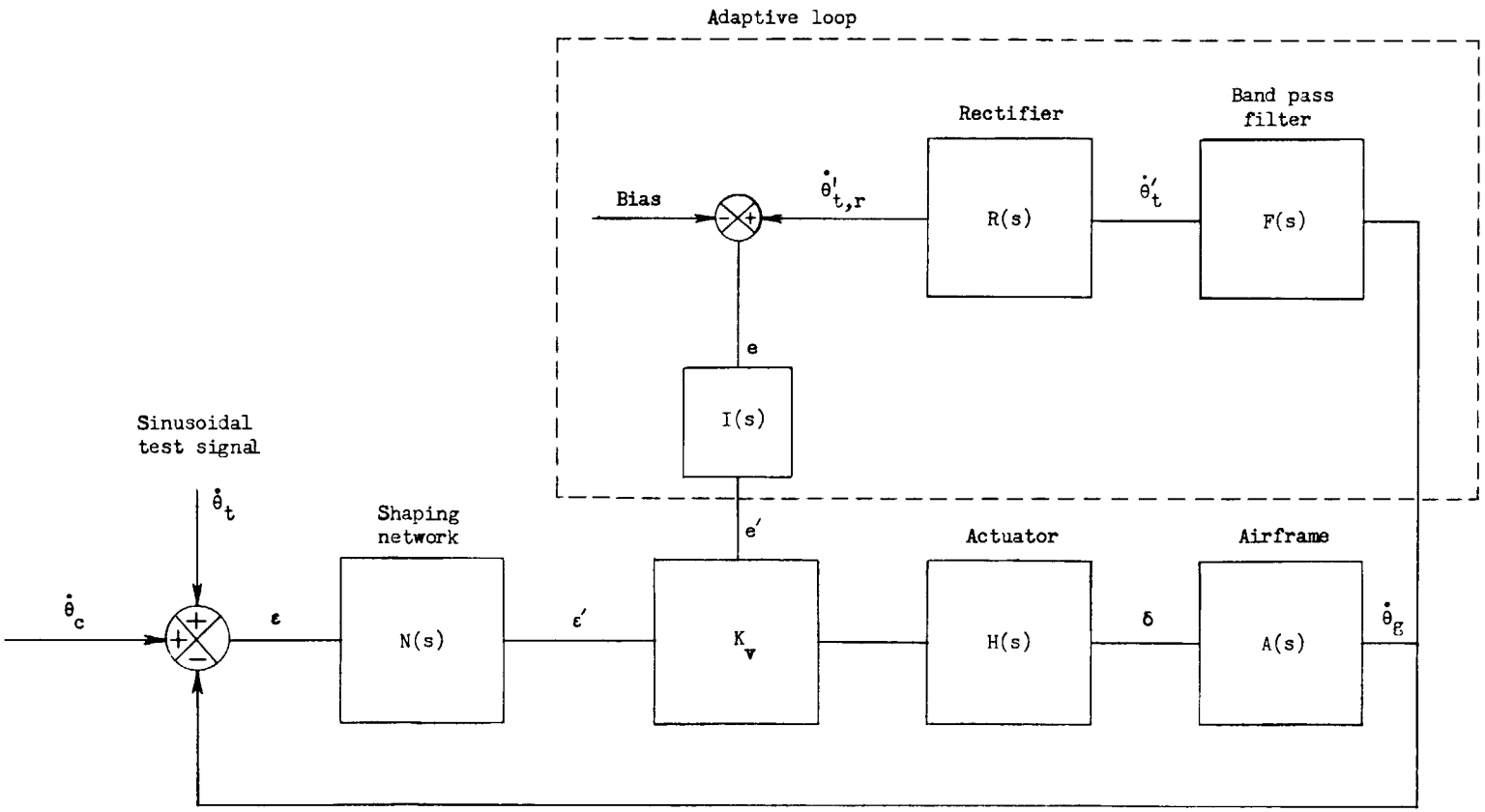

Figure 1.- Adaptive flight-control system.

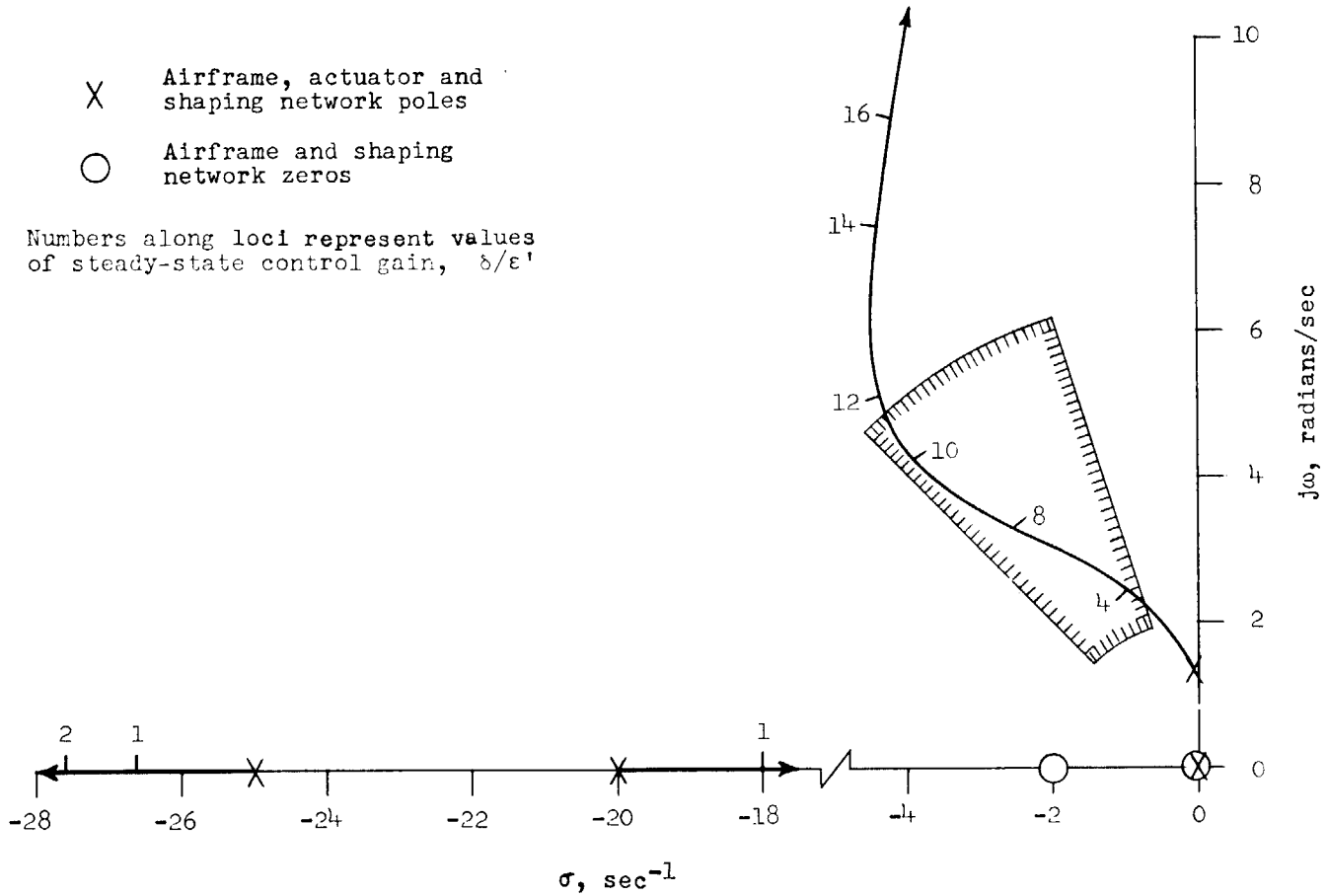

(a) Mach number, 5.8; altitude, 150,000 ft; ω_s = 1.26 radians/sec; ζ_s = 0.075; τ_a = 0.01 sec; and q = 1,970 lb/sq ft.

Figure 2.- Root locus of closed-loop adaptive control system-aircraft characteristics as a function of control gain.

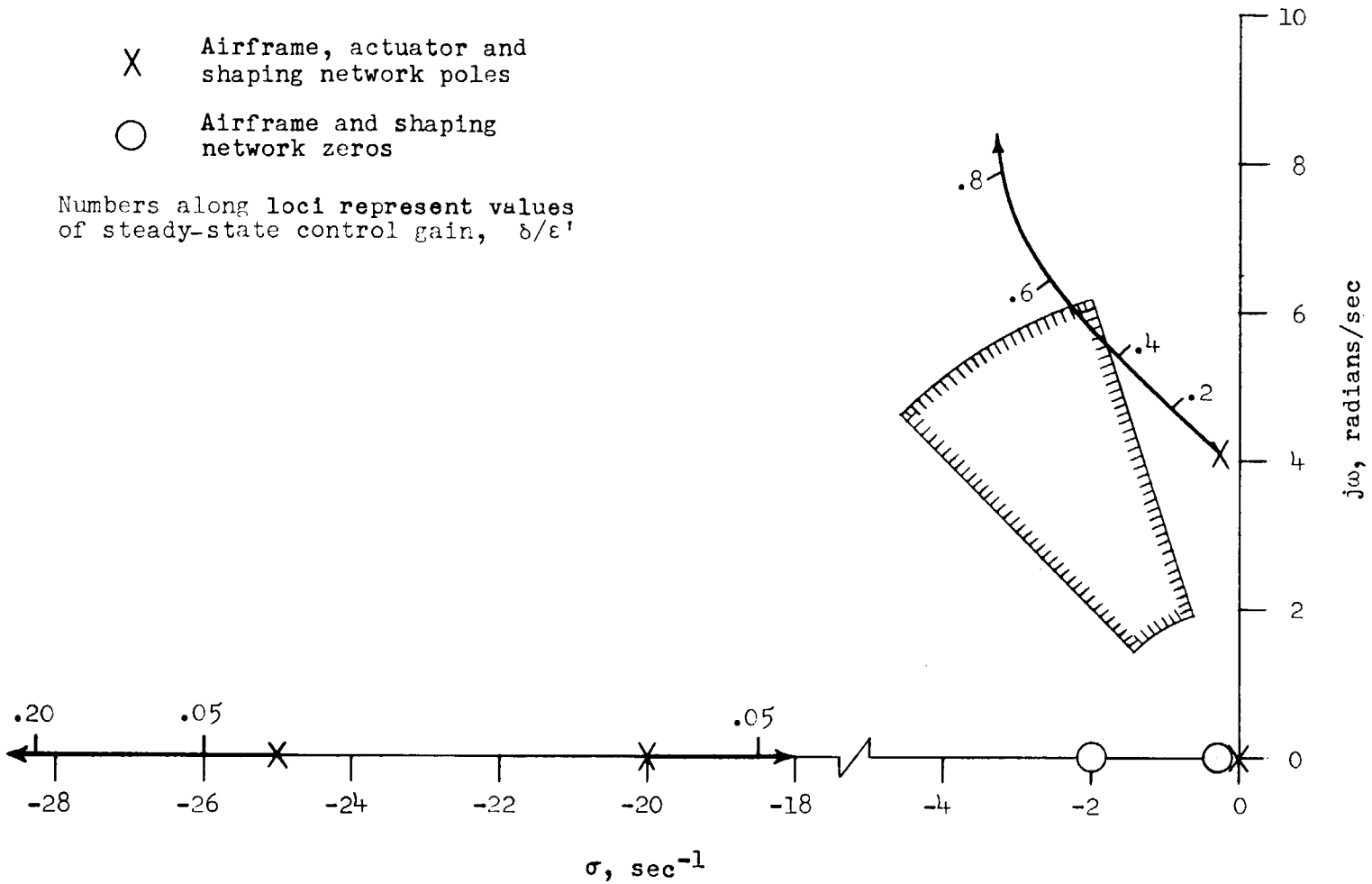

(b) Mach number, 5.5; altitude, 70,000 ft; ω_s = 4.085 radians/sec; ζ_s = 0.065; τ_a = 0.256; and q = 70 lb/sq ft.

Figure 2.- Continued.

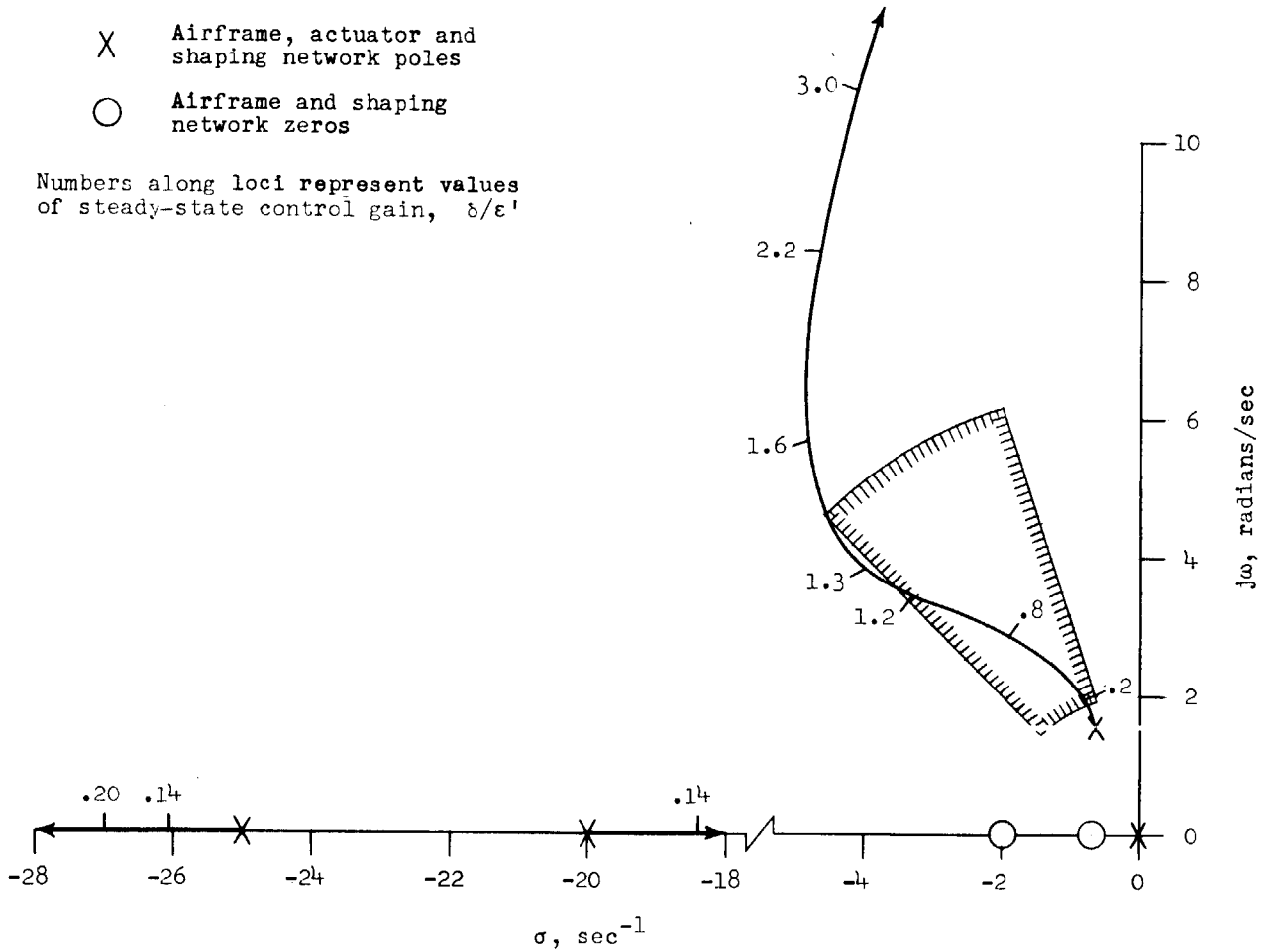

(c) Mach number, 0.5; altitude, 20,000 ft; ω_s = 1.69 radians/sec; ζ_s = 0.382; τ_a = 0.764 sec; and q = 175 lb/sq ft.

Figure 2.- Concluded.

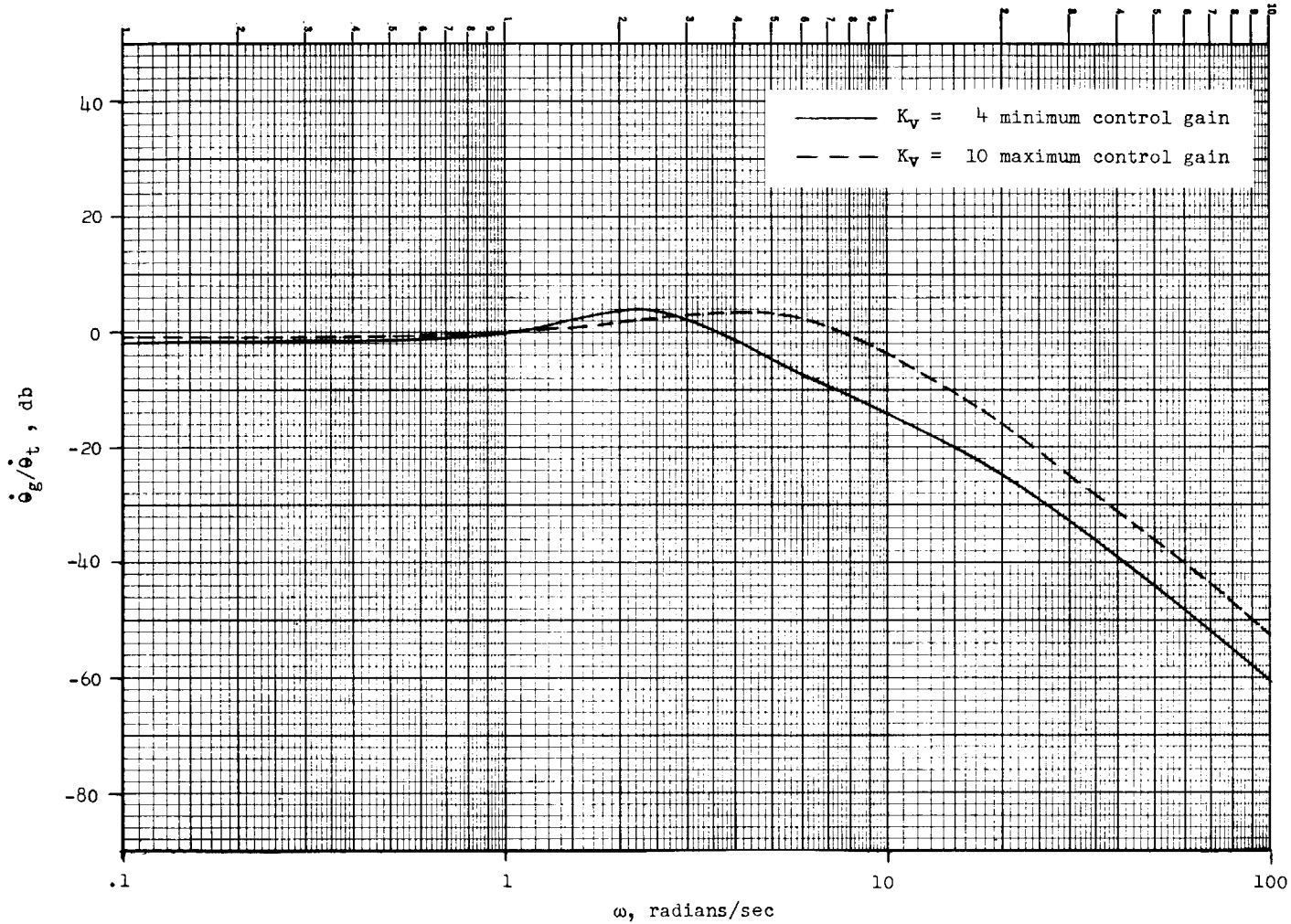

(a) Mach number, 5.8; altitude, 150,000 ft.

Figure 3.- Closed-loop frequency responses of adaptive pitch-rate aircraft control system at maximum and minimum acceptable control loop gain values for three flight conditions.

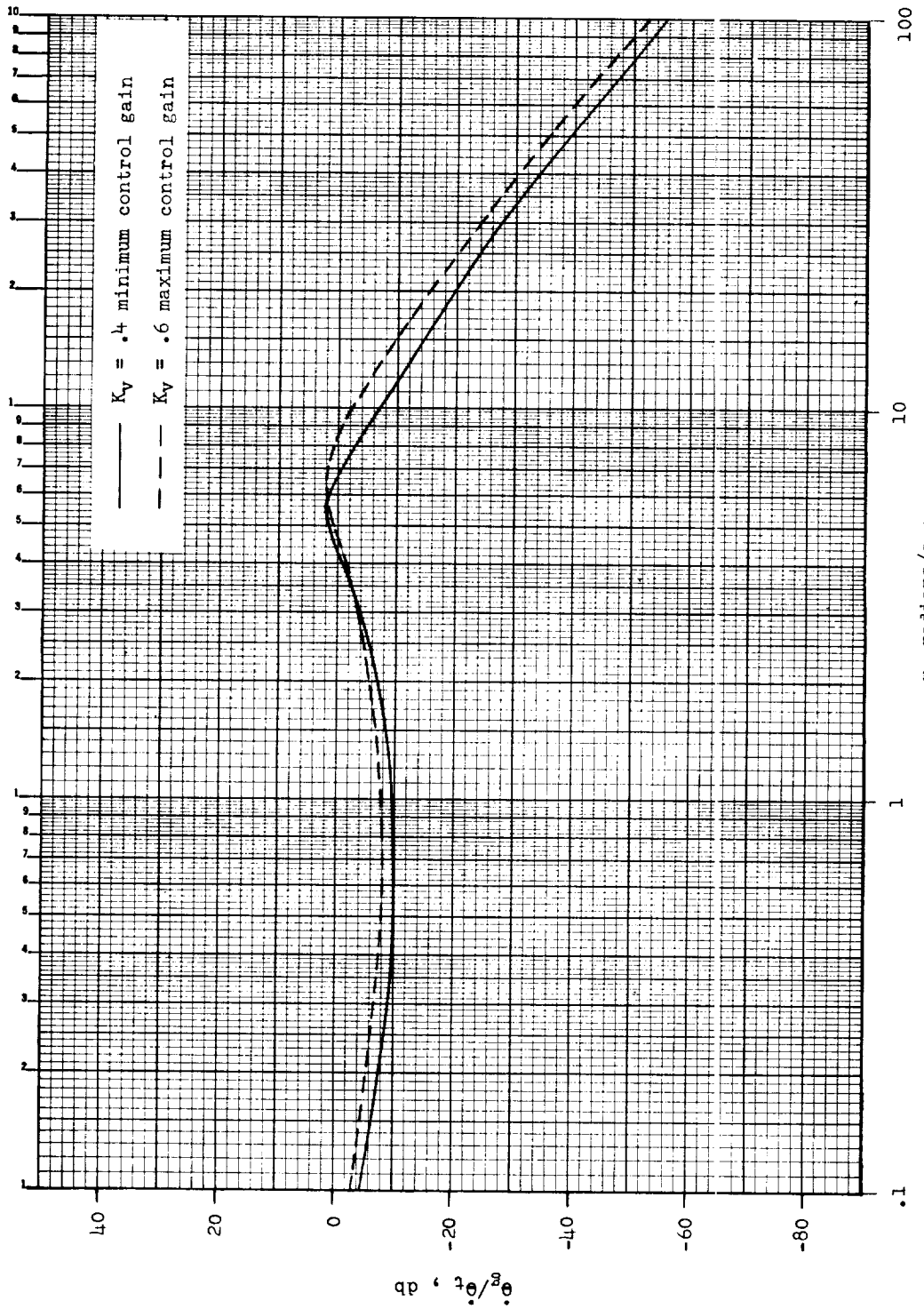

(b) Mach number, 5.5; altitude, 70,000 ft.

Figure 3.- Continued.

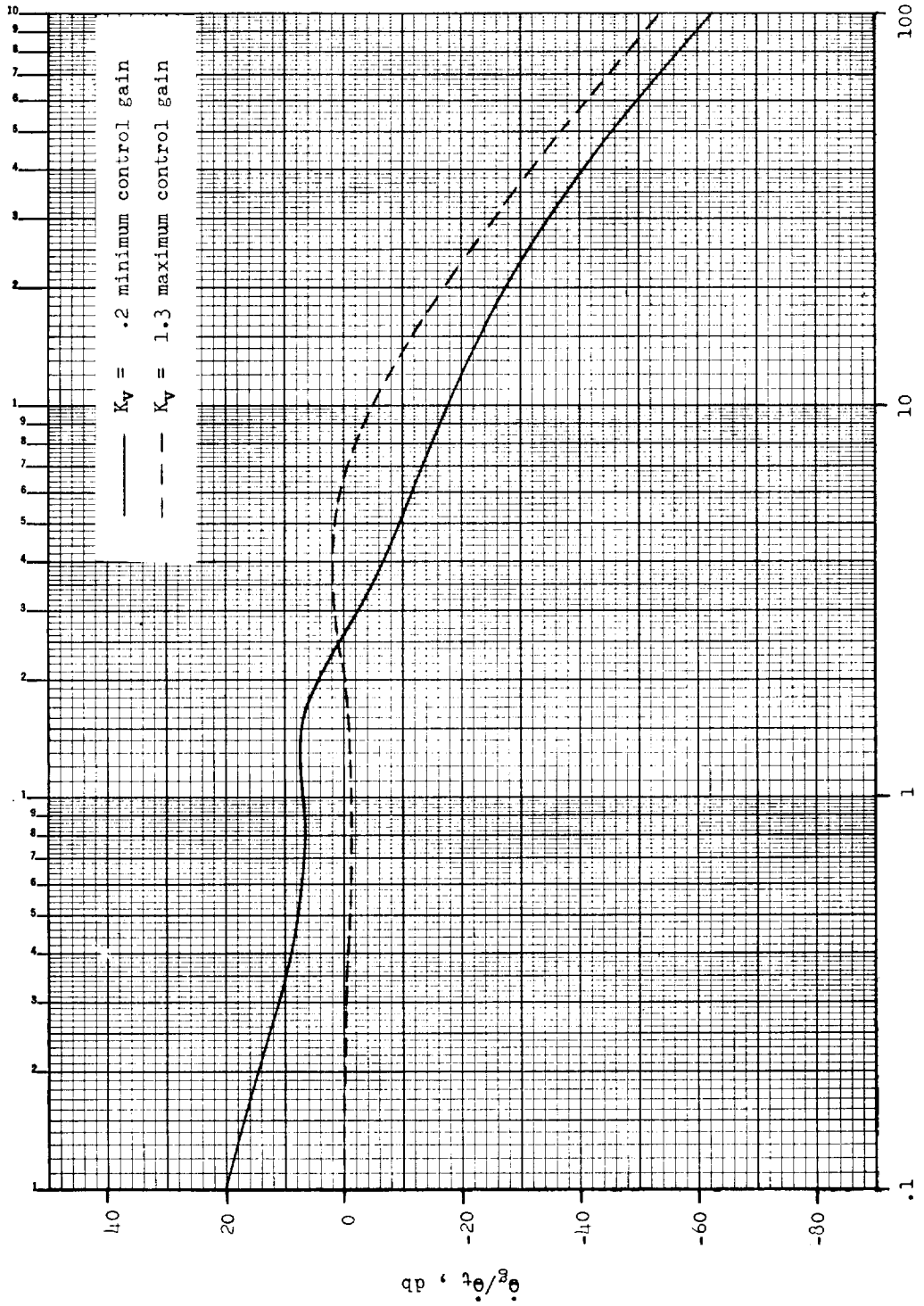

(c) Mach number, 0.5; altitude, 20,000 ft.

Figure 3.- Concluded.

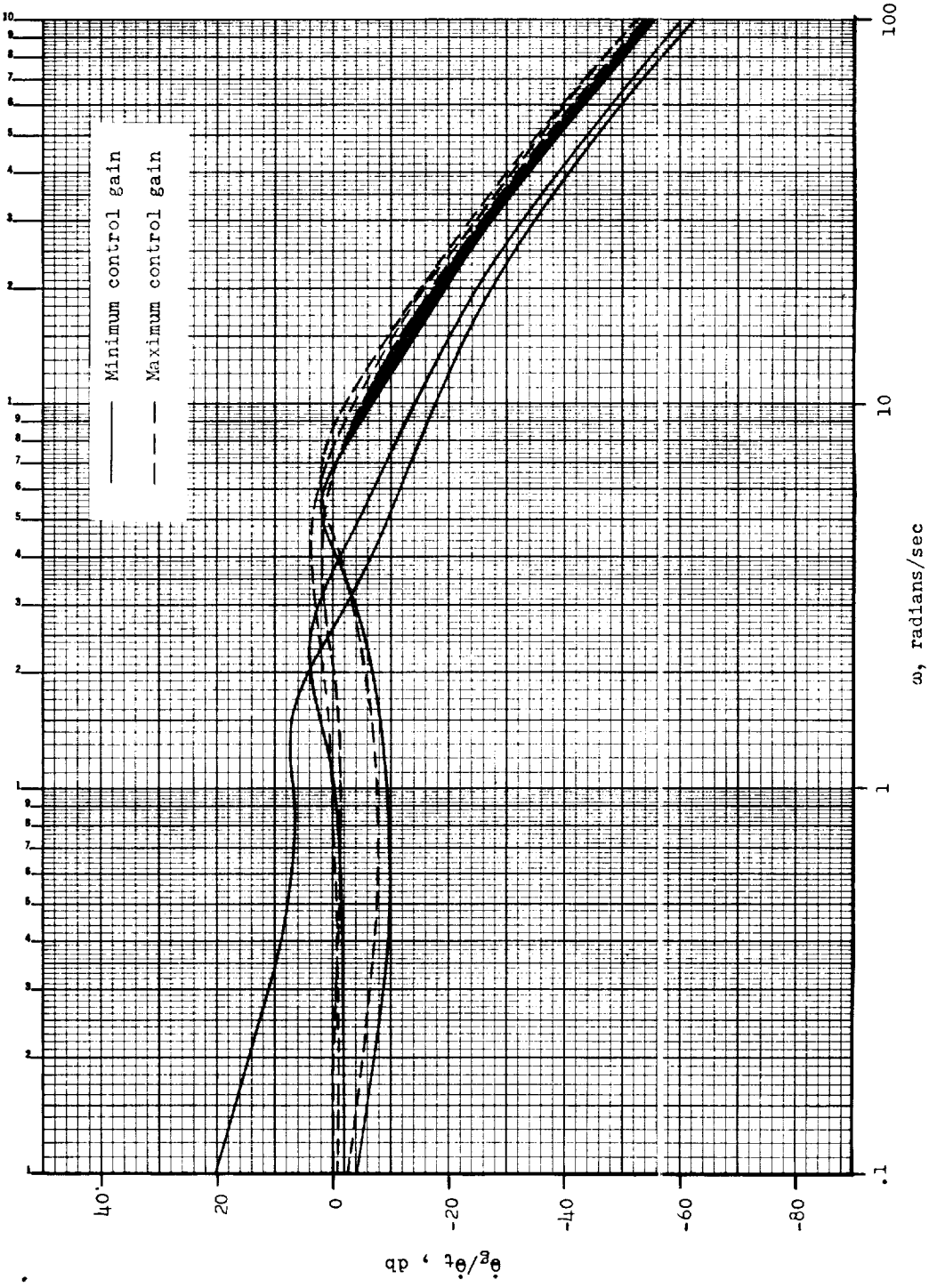

Figure 4.- Frequency region of common $\dot{\theta}_t/\dot{\theta}_g$ ratios for adaptive aircraft control system as determined by superposition of frequency response plots of figures 3(a), 3(b), and 3(c).

L-1470

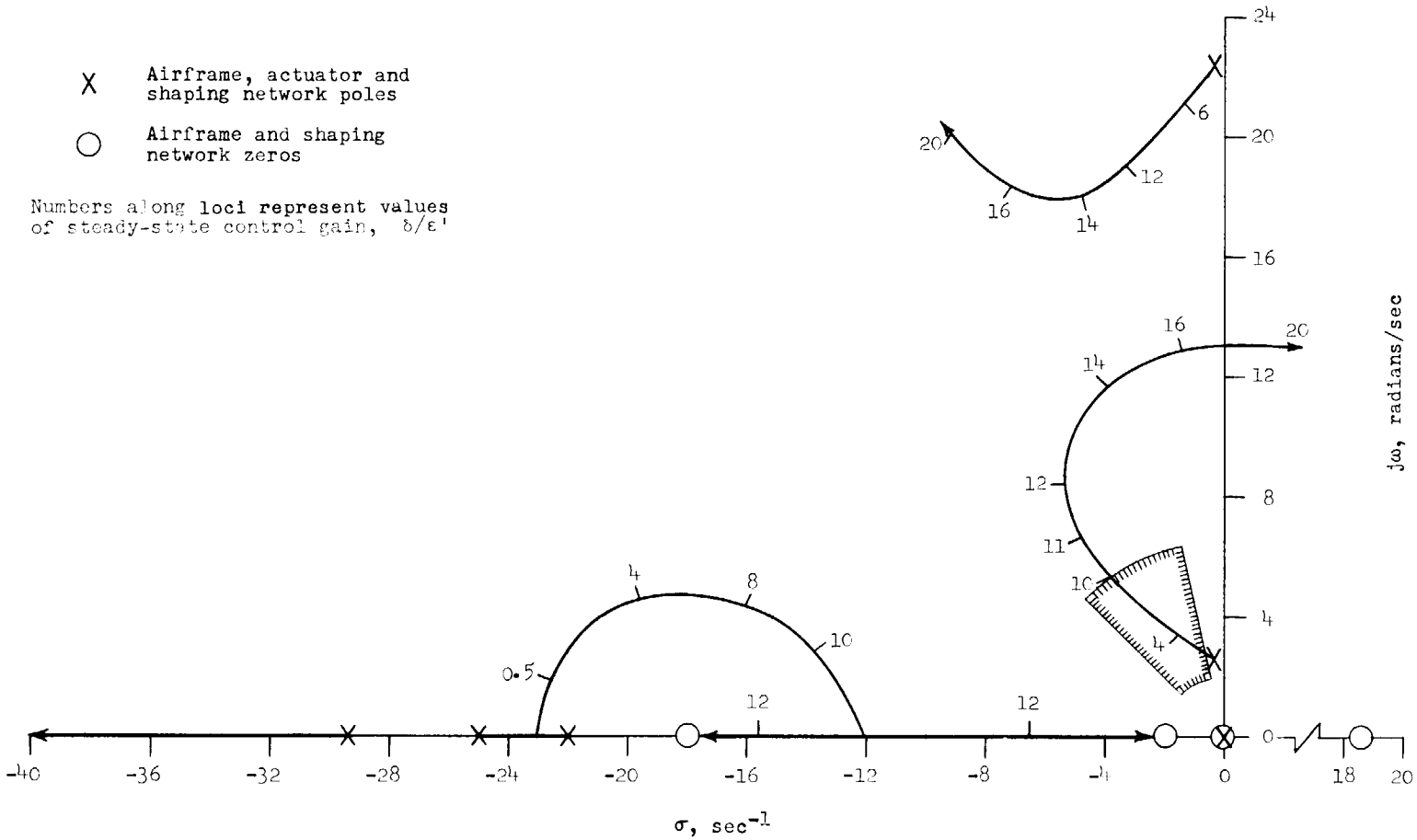

(a) Mach number, 1; altitude, 5,000 ft.; rate sensor station 646; ω_s = 2.7 radians/sec; ζ_s = 0.08; ω_b = 22.4 radians/sec; ζ_b = 0.01; τ_a = 0.056 sec; and q = 8.5 lb/sq in.

Figure 5.- Root locus of closed-loop adaptive control system-missile characteristics as a function of control gain.

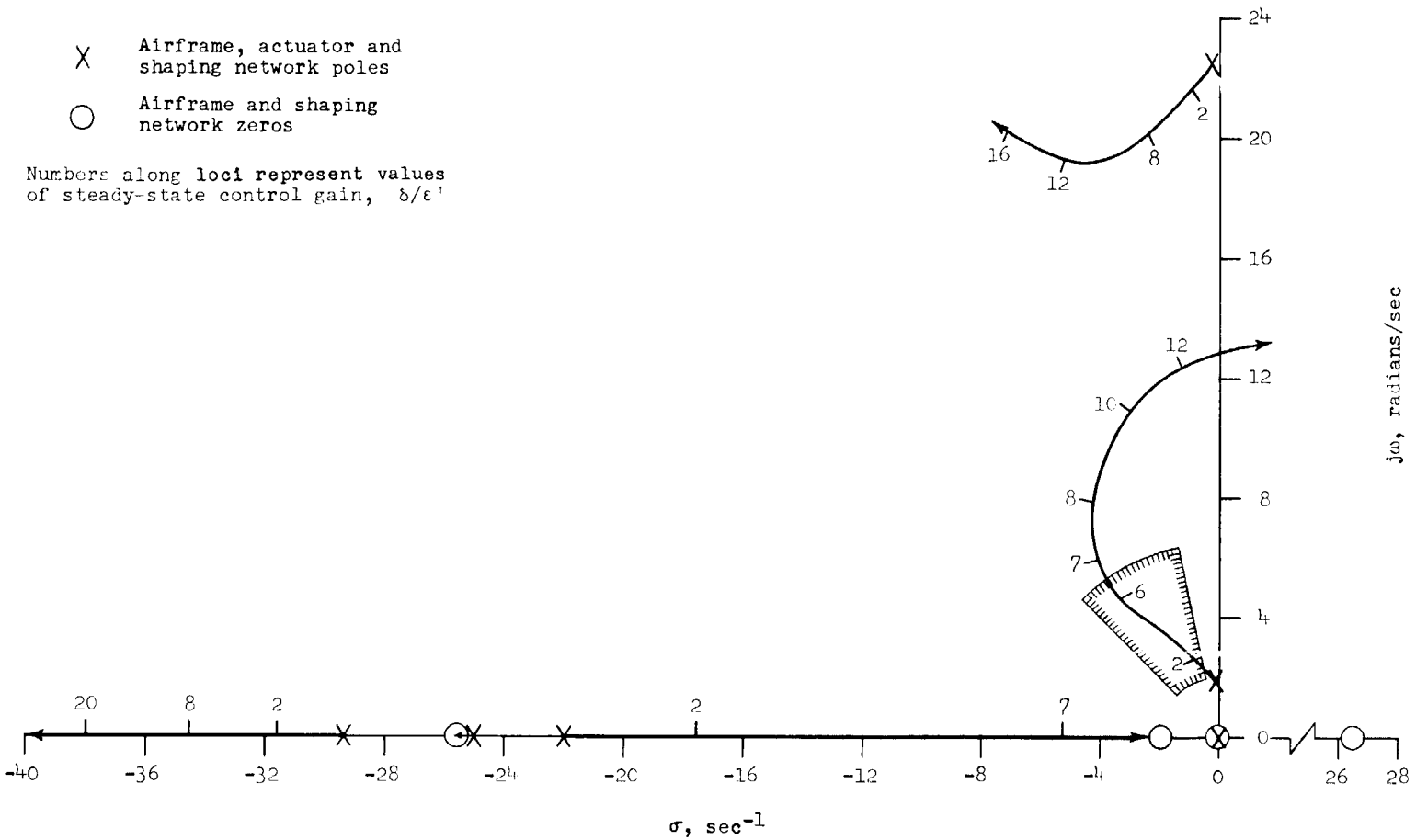

(b) Mach number, 3.25; altitude, 35,000 ft; rate sensor station 646; ω_s = 1.9 radians/sec; ζ_s = 0.08; ω_b = 22.4 radians/sec; ζ_b = 0.01; τ_a = 0.935 sec; and q = 31.4 lb/sq in.

Figure 5.- Continued.

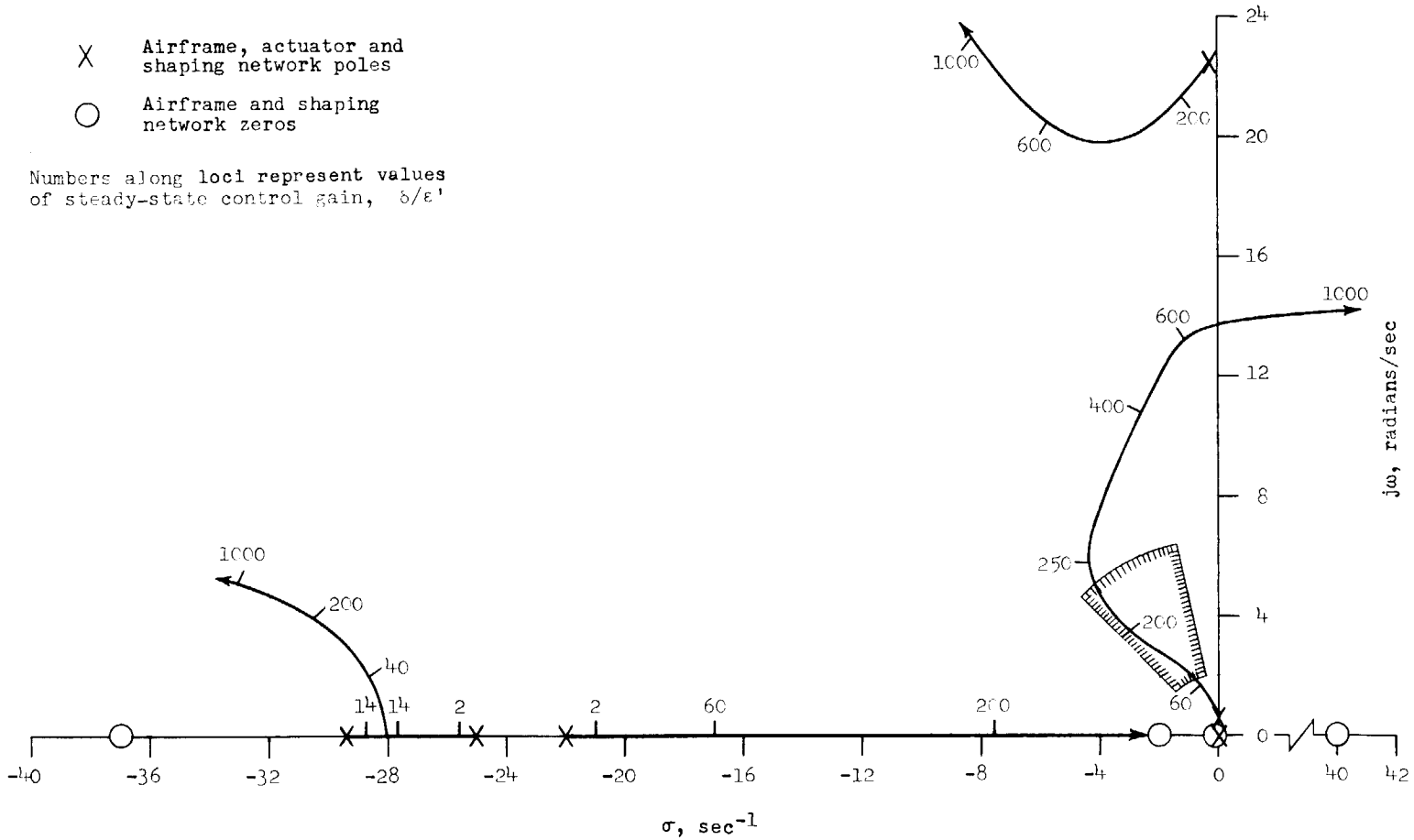

(c) Mach number, 3.6; altitude, 100,000 ft; rate sensor station 646; ω_s = 0.57 radian/sec; ζ_s = 0.0158; ω_b = 22.4 radians/sec; ζ_b = 0.01; τ_a = 0.00435 sec; and q = 1.5 lb/sq in.

Figure 5.- Continued.

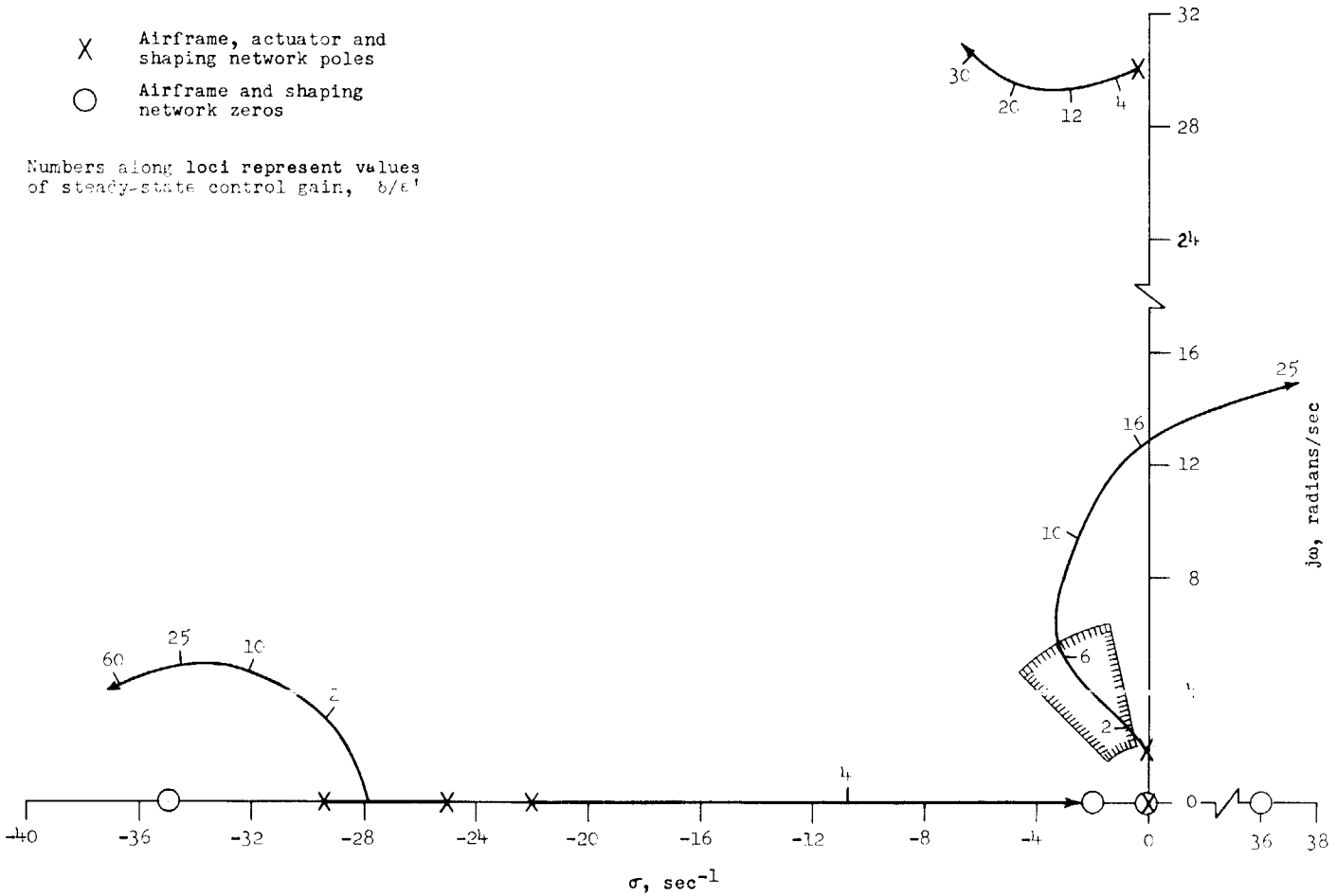

(d) Mach number, 3.25; altitude, 35,000 ft; rate sensor station 646; ω_s = 1.9 radians/sec; ζ_s = 0.08; ω_b = 30 radians/sec; ζ_b = 0.01; τ_a = 0.11 sec; and q = 31.4 lb/sq in.

Figure 5.- Continued.

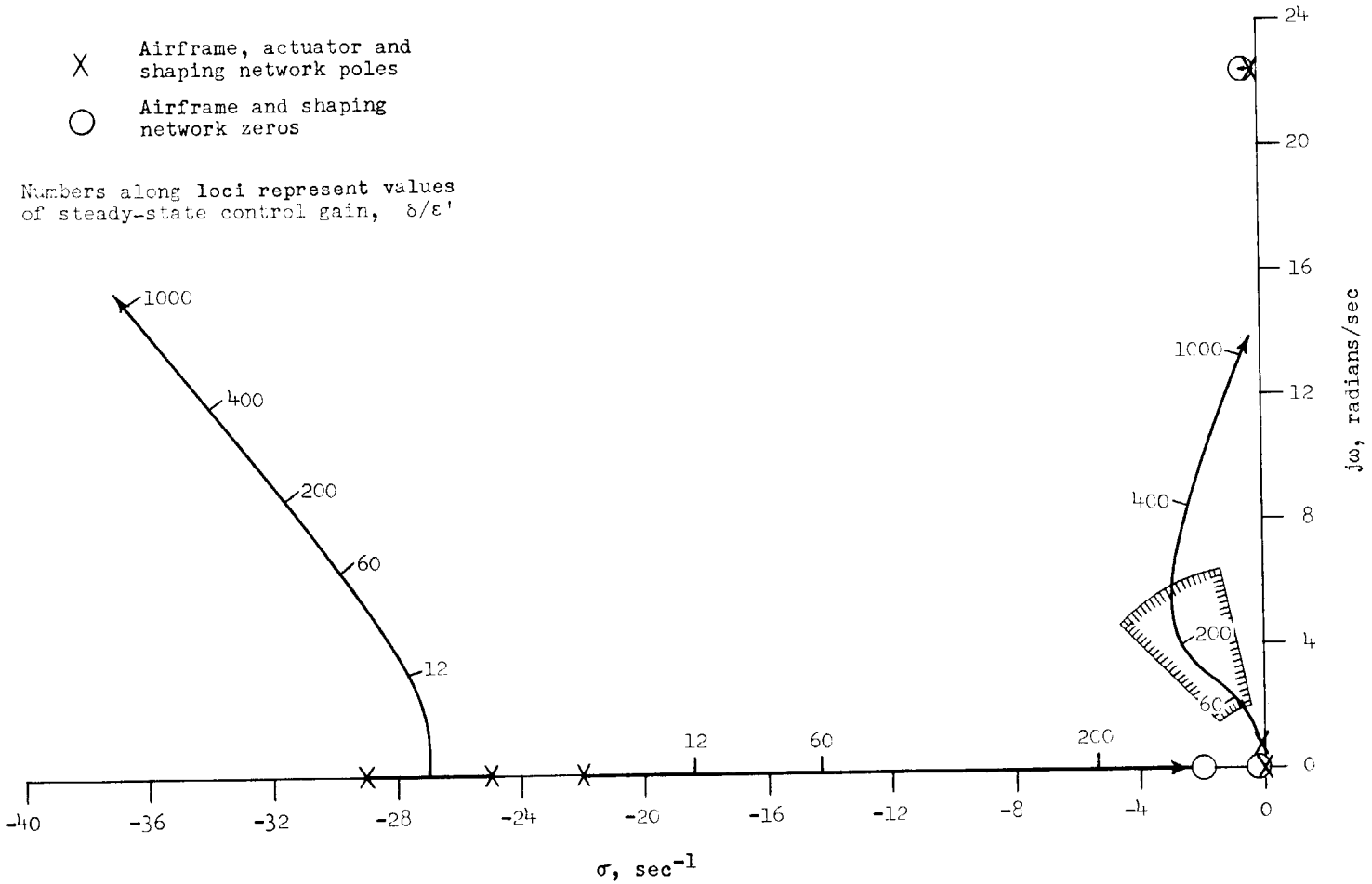

(e) Mach number, 3.6; altitude, 100,000 ft; rate sensor station 400; ω_s = 0.57 radian/sec; ζ_s = 0.0158; ω_b = 22.4 radians/sec; ζ_b = 0.01; τ_a = 0.00435 sec; and q = 1.5 lb/sq in.

Figure 5.- Concluded.

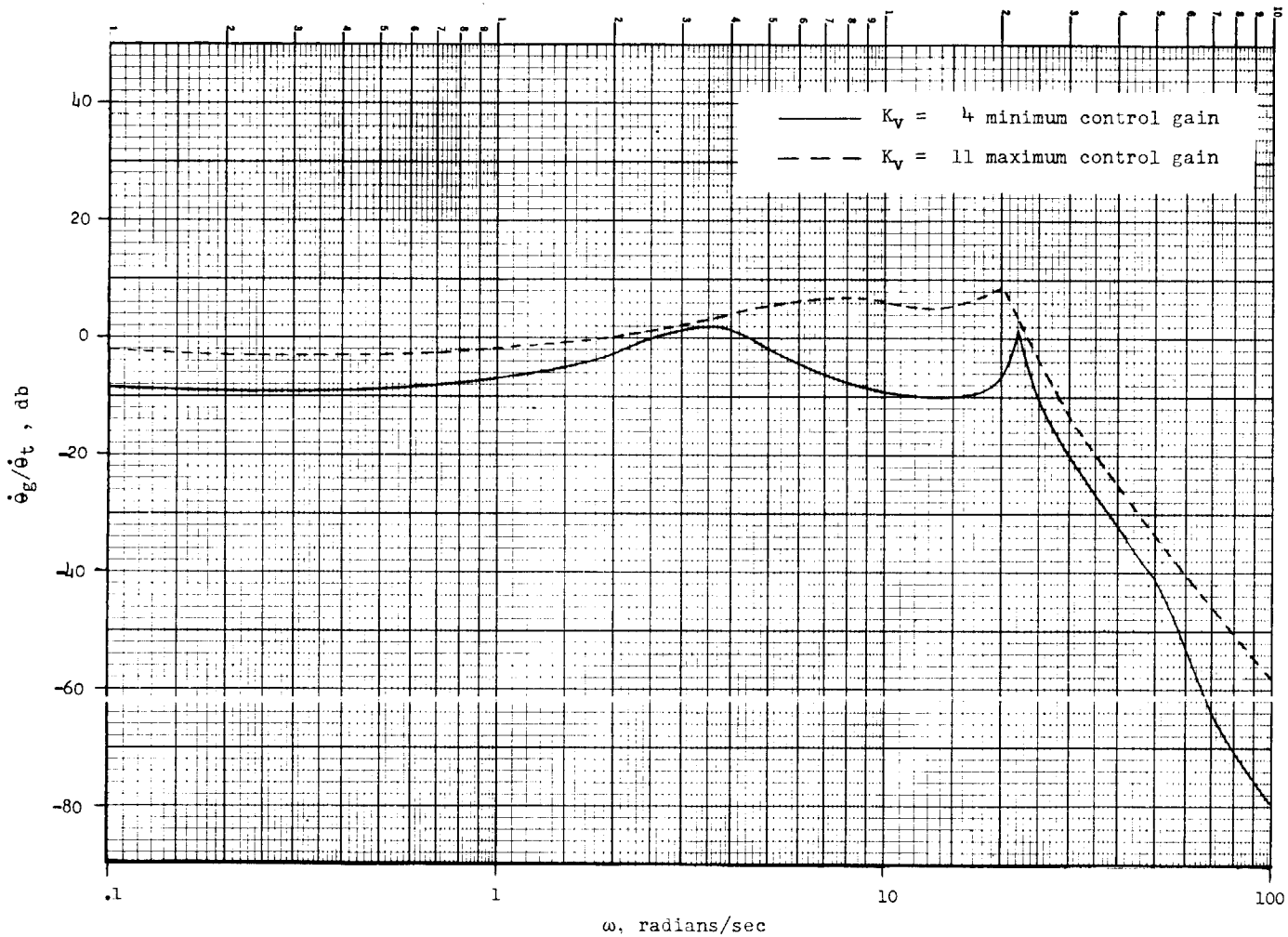

(a) Mach number, 1; altitude, 5,000 ft.

Figure 6.- Closed-loop frequency responses of adaptive pitch-rate missile control system at maximum and minimum acceptable control-loop gain values for three flight conditions.

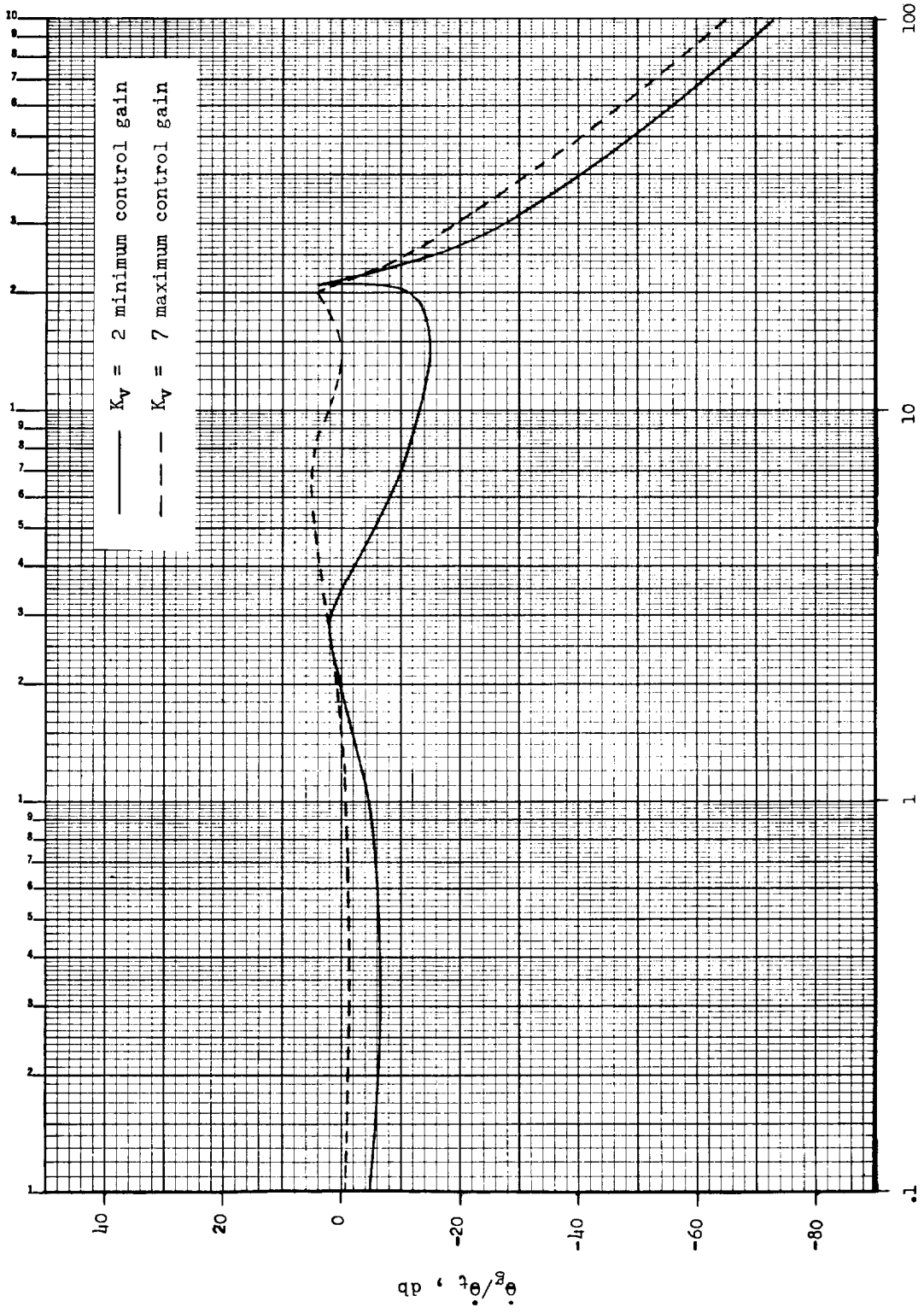

(b) Maximum value of q, altitude of 35,000 ft.

Figure 6.- Continued.

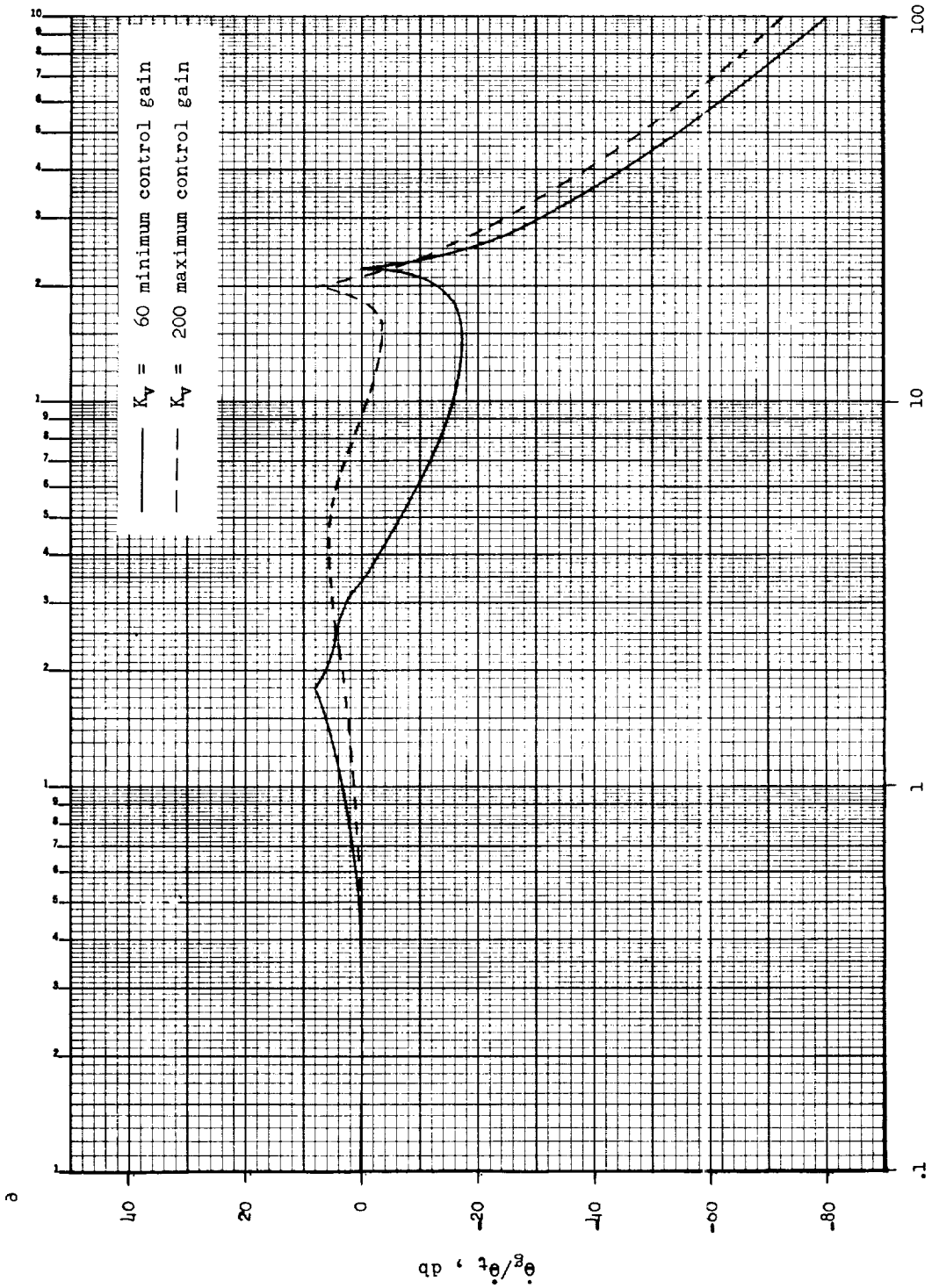

(c) At 19 seconds after burmout, altitude 100,000 ft.

Figure 6.- Concluded.

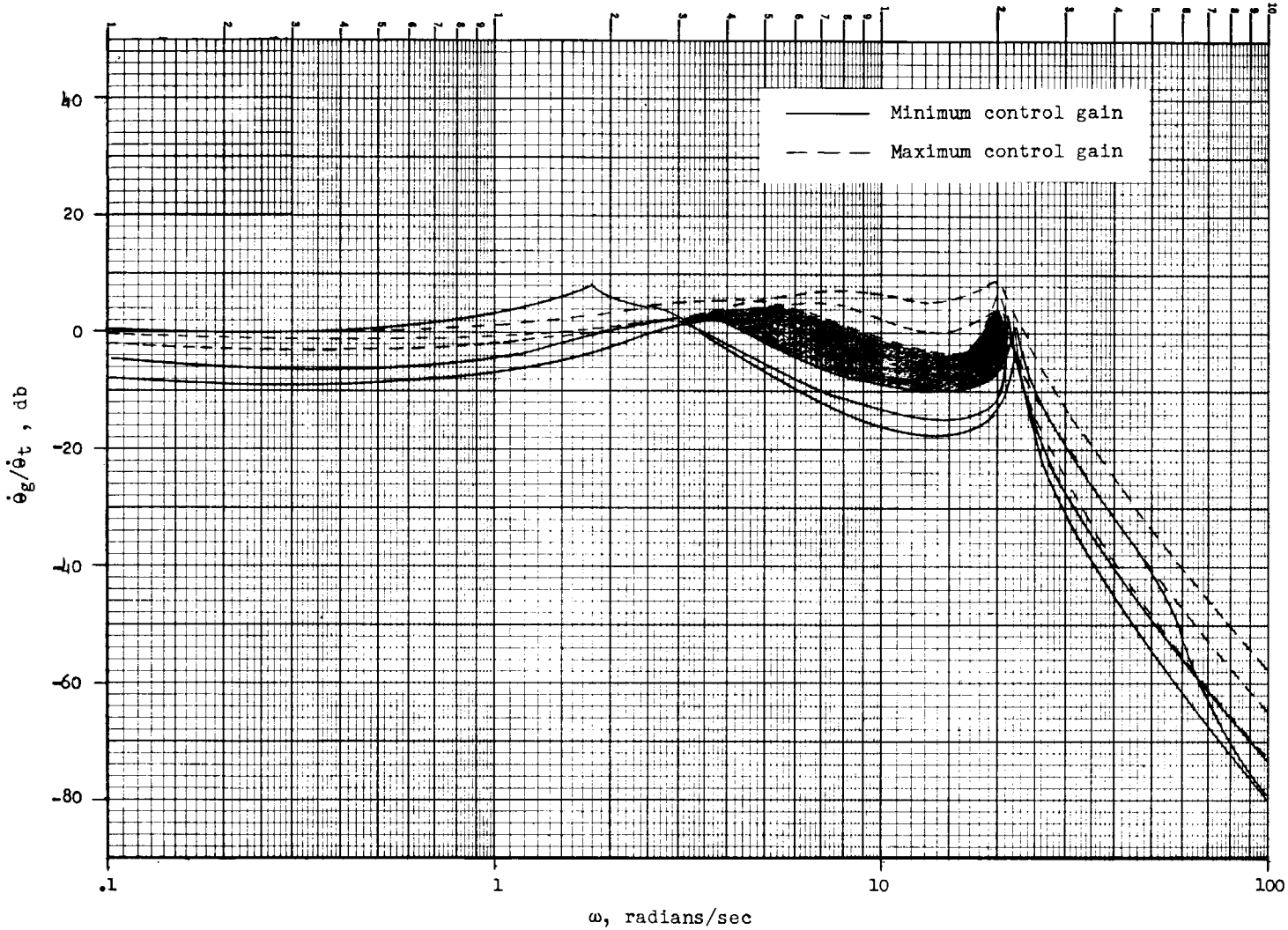

Figure 7.- Frequency region of common $\dot{\theta}_t/\dot{\theta}_g$ ratios for adaptive missile control system as determined by superposition of frequency response plots of figures 6(a), 6(b), and 6(c).

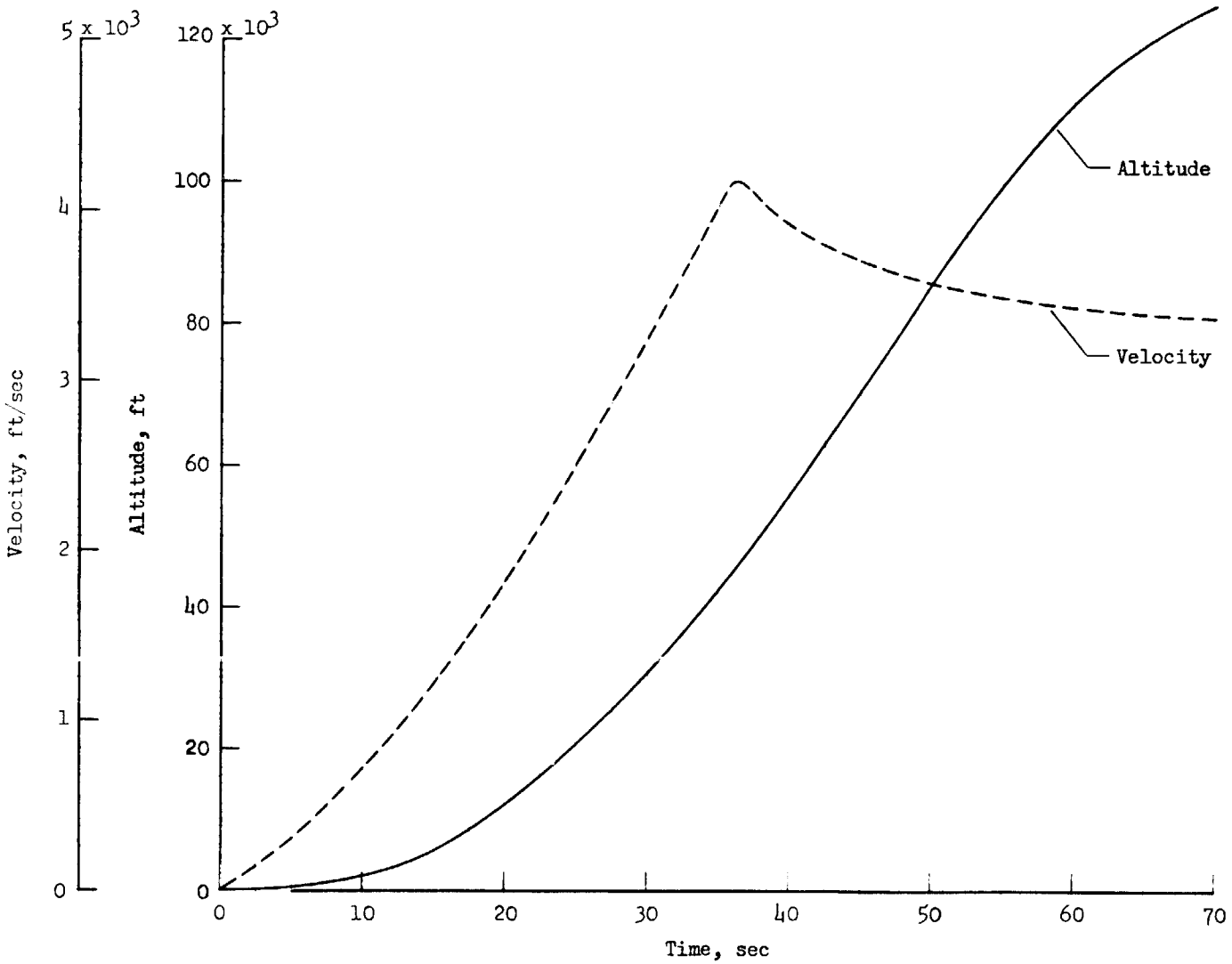

Figure 8.- Missile trajectory characteristics.

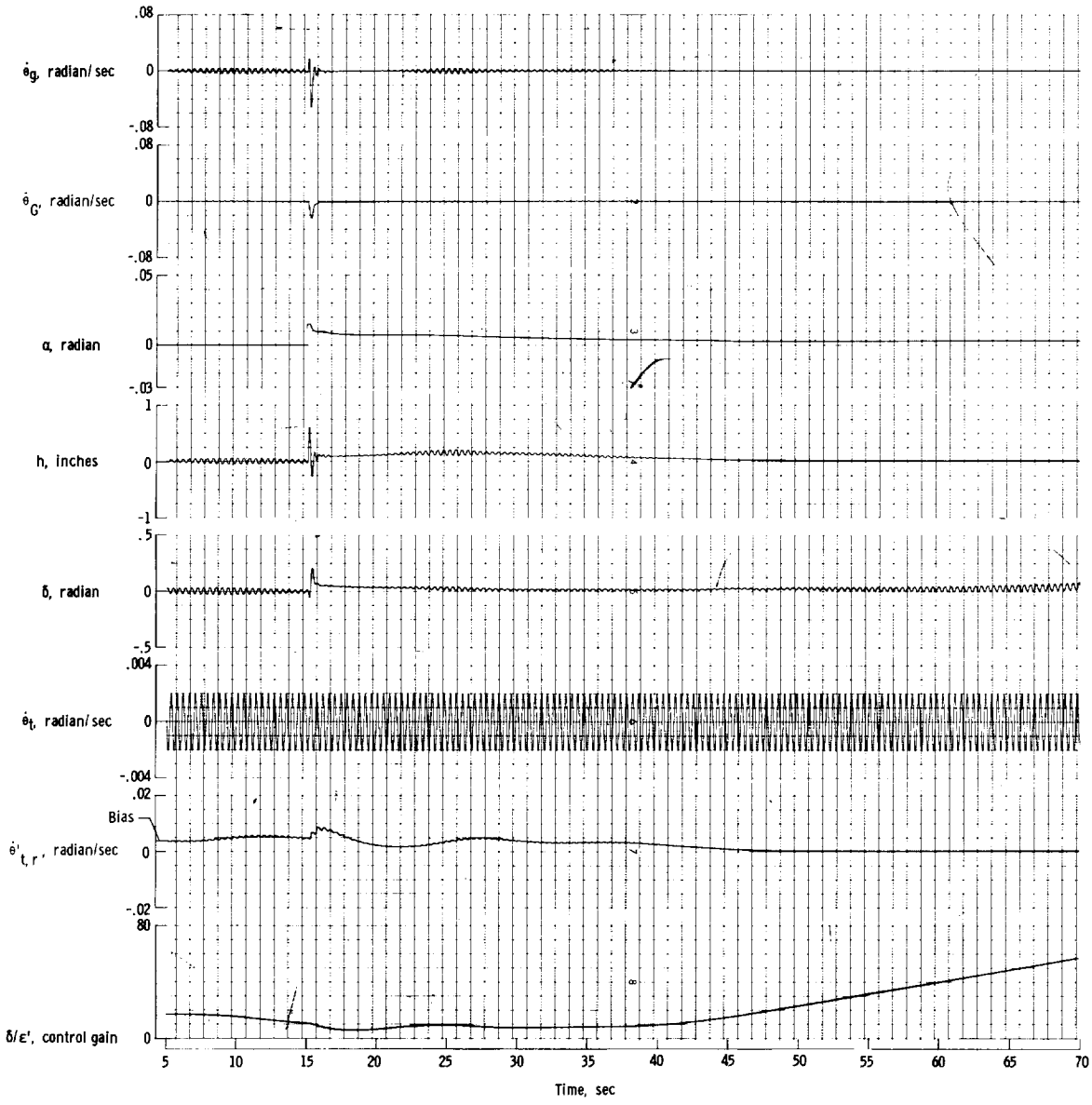

(a) Band-pass filter 0.05; disturbance, 21 ft/sec horizontal-velocity sharp-edge gust initiated at time 15 seconds.

Figure 9.- Adaptive pitch-rate missile-control-system performance; trajectory portion from 5 seconds after launch to second-stage ignition.

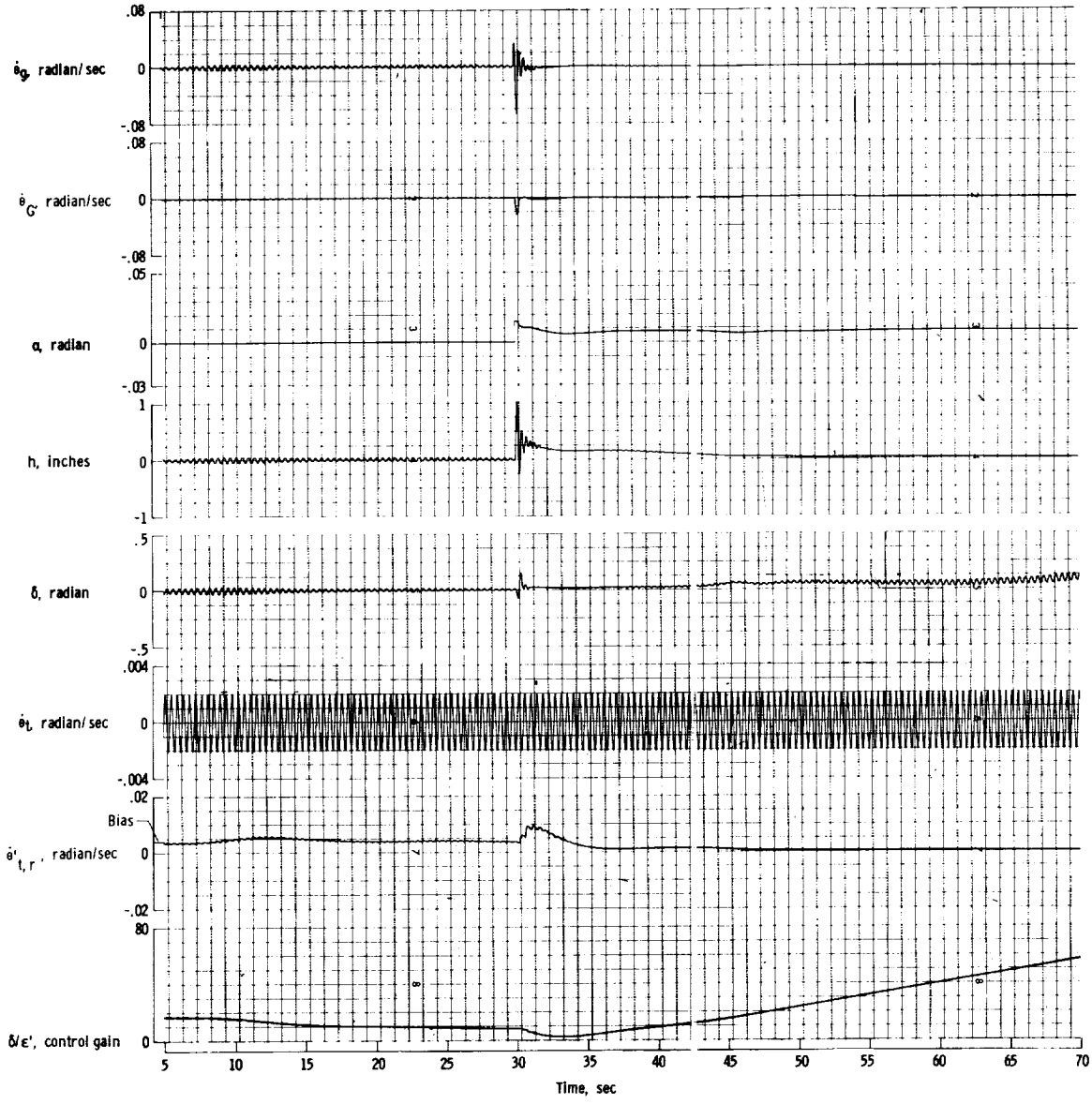

(b) Band-pass filter 0.05; disturbance, 57 ft sec horizontal-velocity sharp-edge gust initiated at time 30 seconds.

Figure 9.- Continued

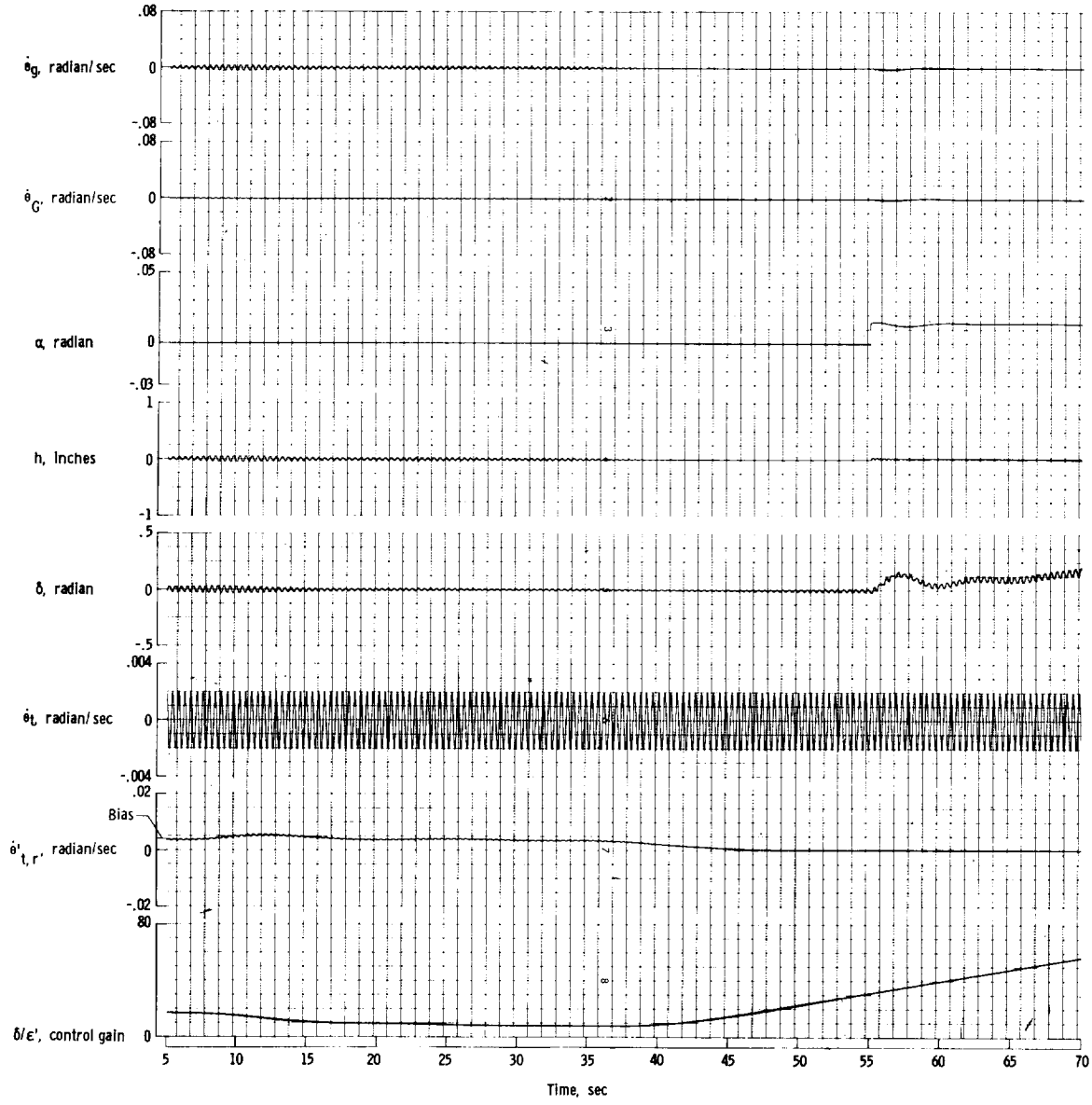

(c) Band-pass filter 0.05; disturbance, 59.5 ft/sec horizontal-velocity sharp-edge gust initiated at time 55 seconds.

Figure 9.- Continued.

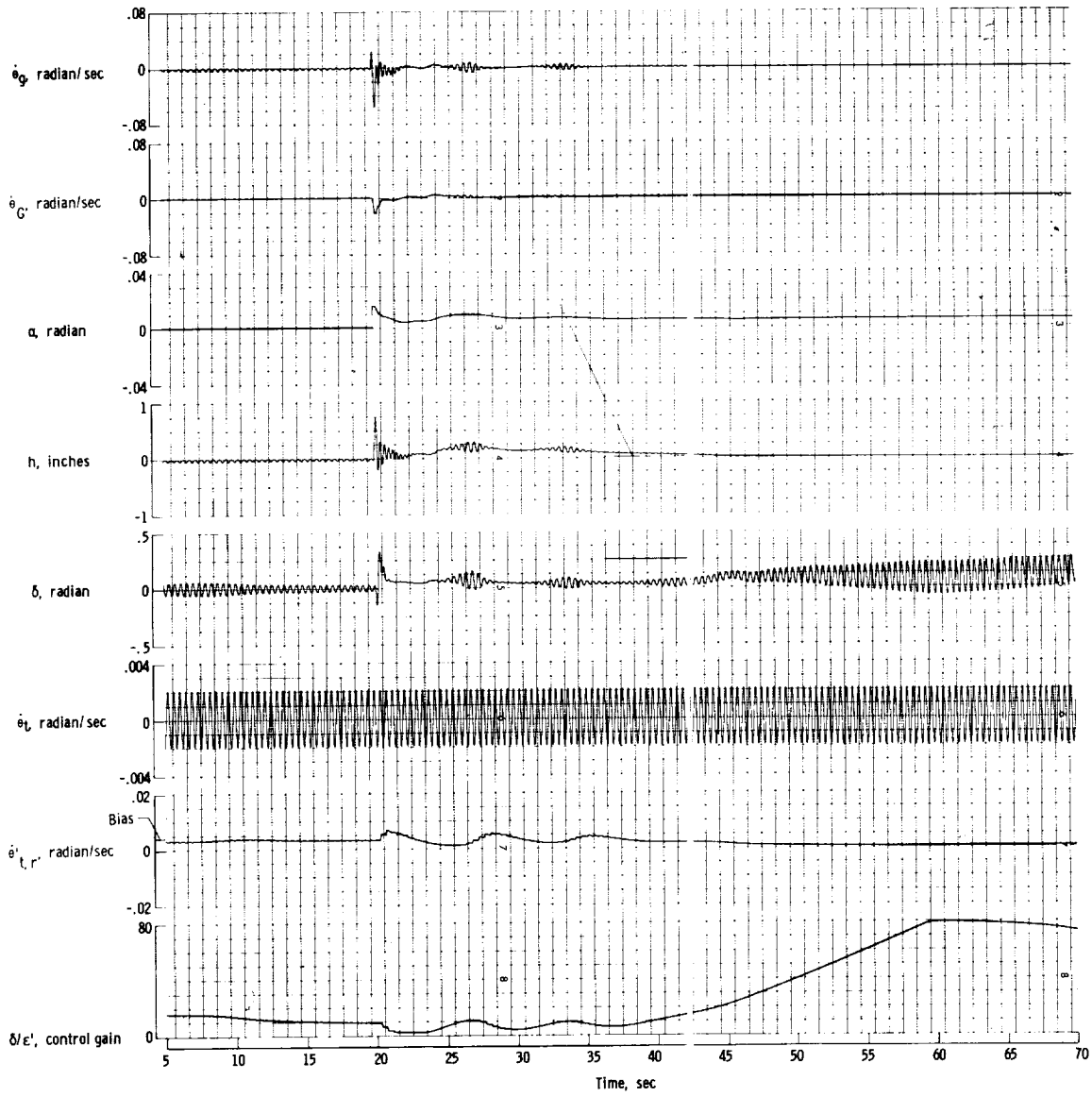

(d) Band-pass filter 0.05 and increased error sensitivity; disturbance, 32 ft/sec horizontal-velocity sharp-edge gust encountered at time 20 seconds.

Figure 9.- Continued.

I-1456

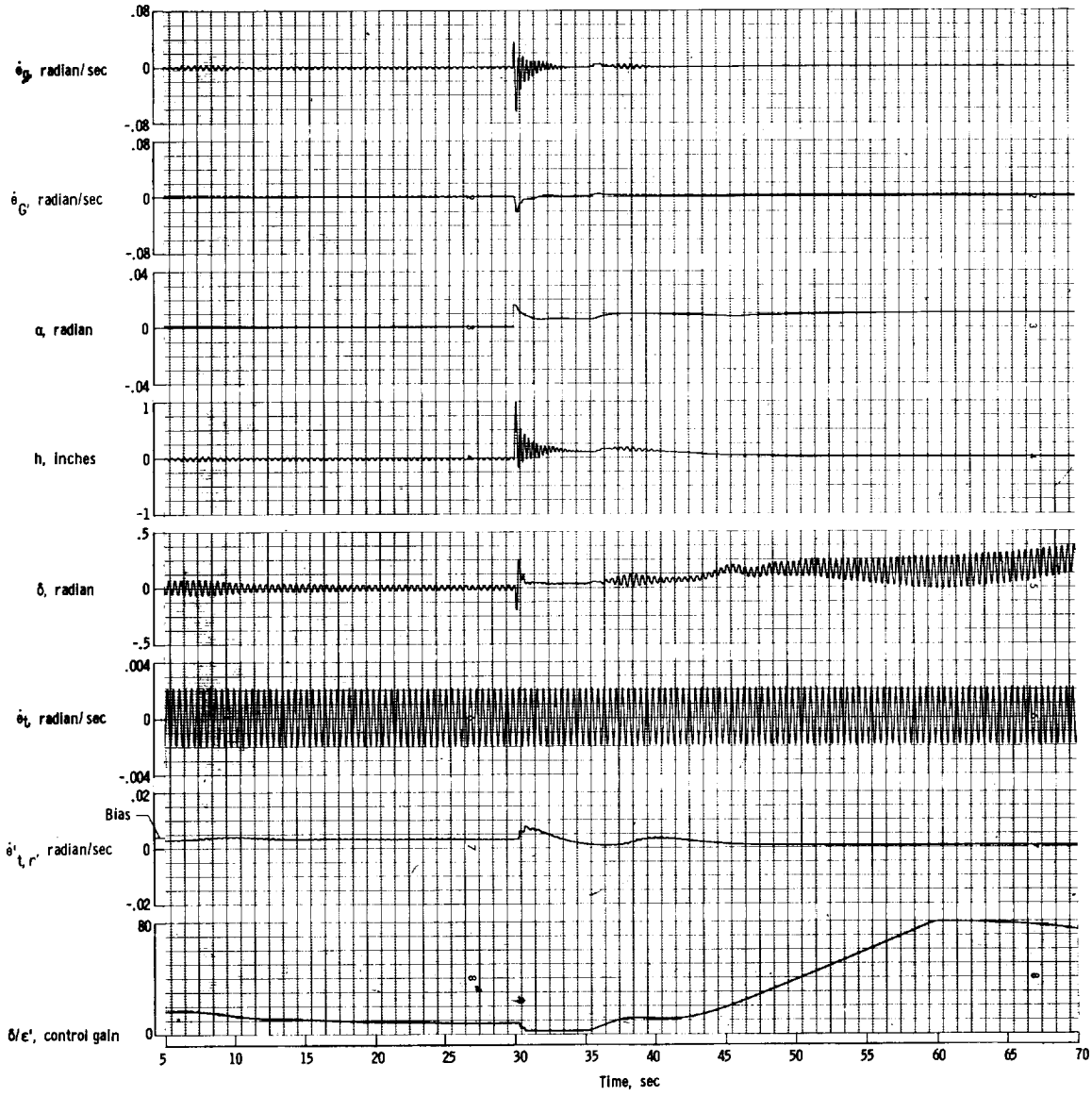

(e) Band-pass filter 0.05 and increased error sensitivity; disturbance, 57 ft/sec horizontal-velocity sharp-edge gust encountered at time 30 seconds.

Figure 9.- Continued.

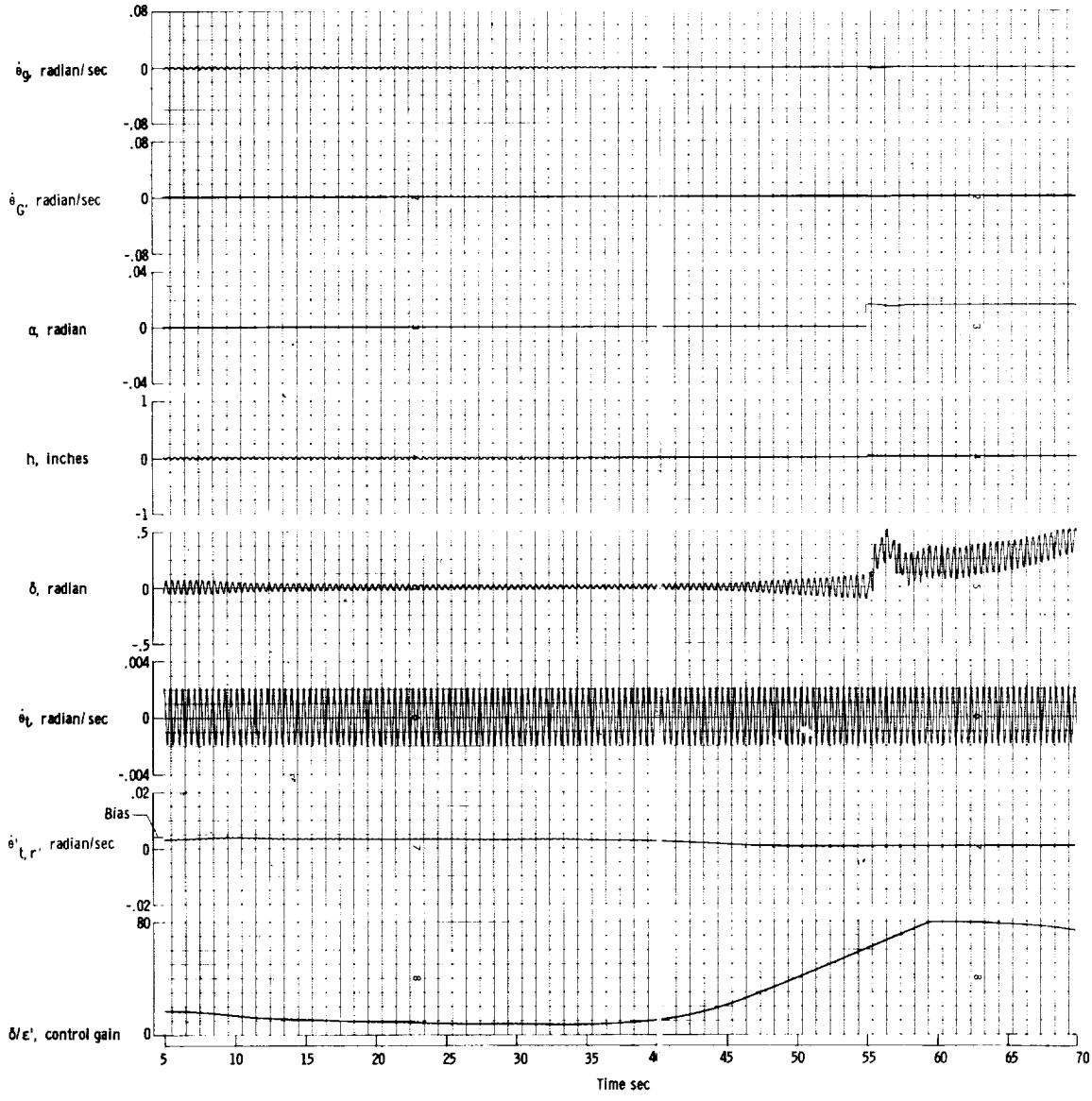

(f) Band-pass filter 0.05 and increased error sensitivity; disturbance, 59.5 ft/sec horizontal-velocity sharp-edge gust encountered at time 55 seconds.

Figure 9.- Continued.

L-14536

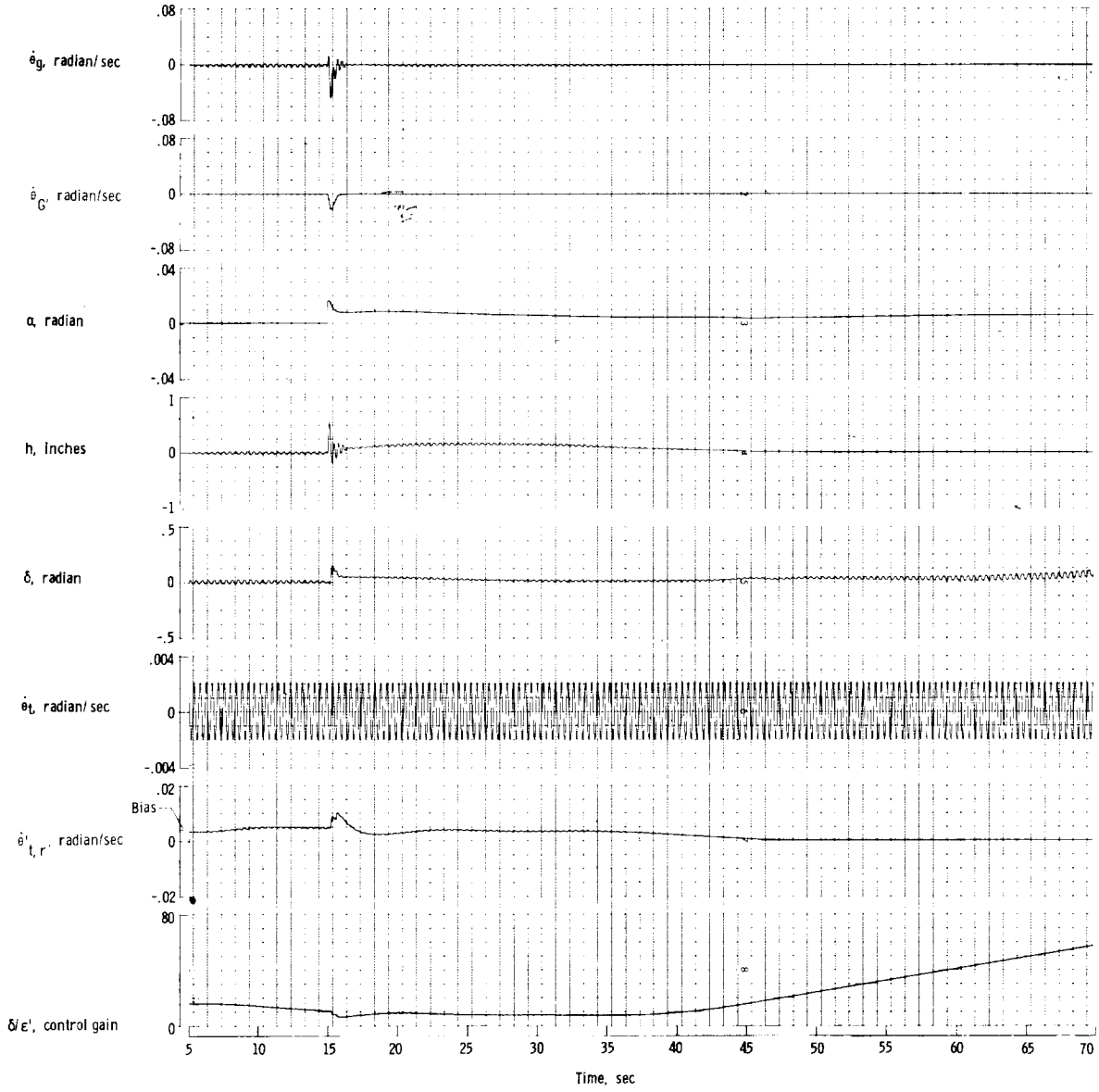

(g) Band-pass filter 0.1; disturbance, 21 ft/sec horizontal-velocity sharp-edge gust initiated at time 15 seconds.

Figure 9.- Continued.

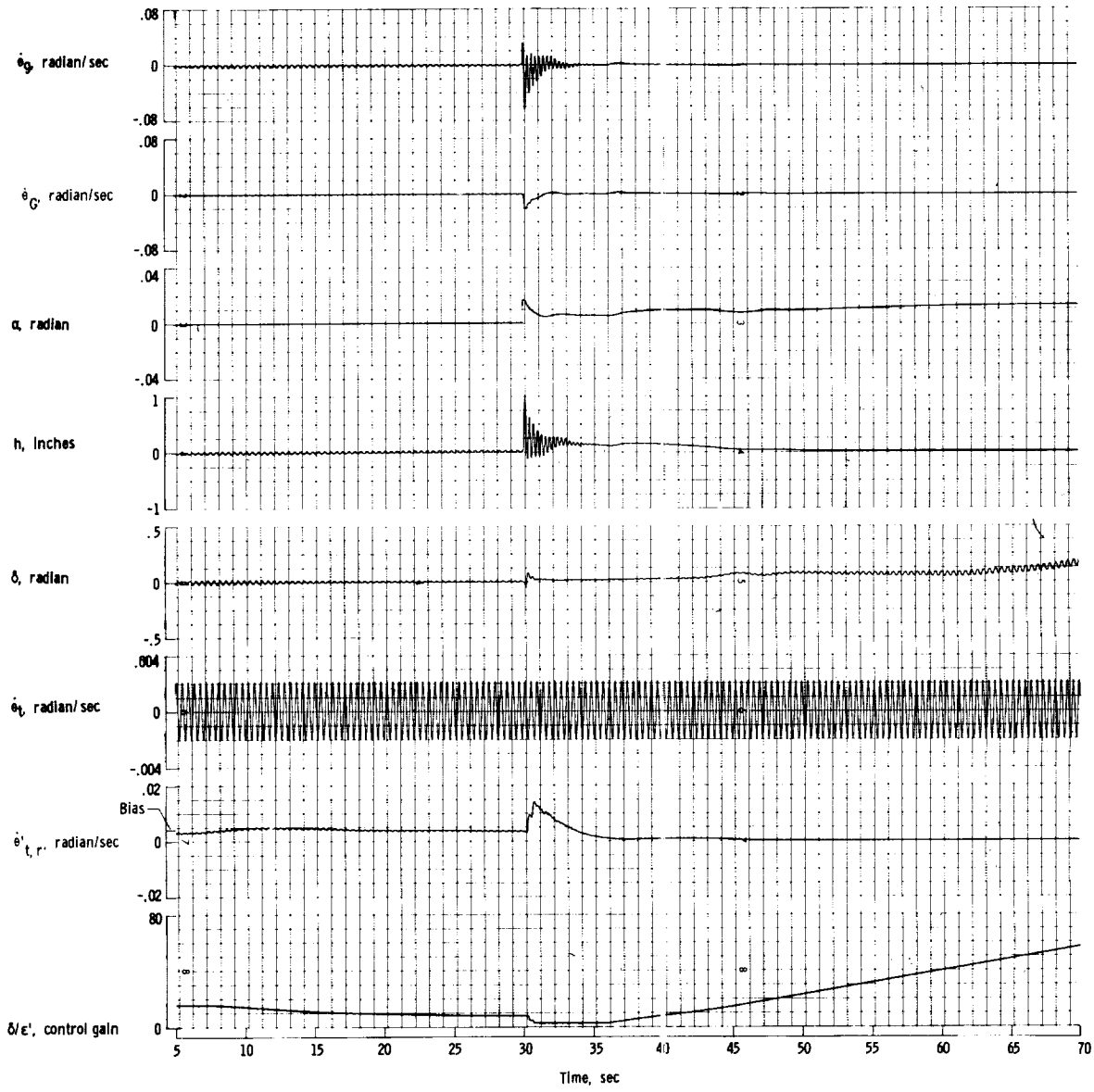

(h) Band-pass filter 0.1; disturbance, 57 ft/sec horizontal-velocity sharp-edge gust initiated at time 30 seconds.

Figure 9.- Continued.

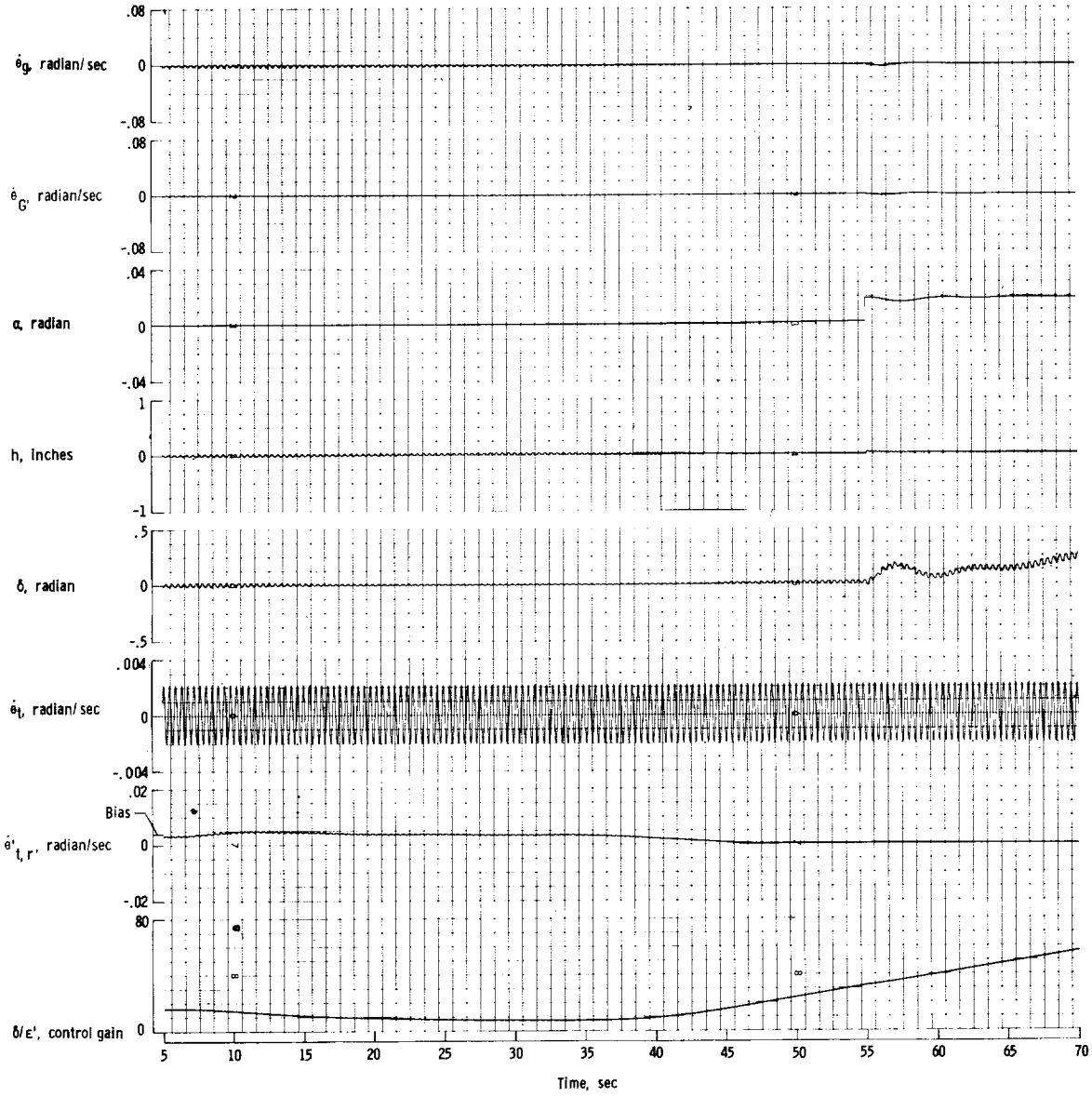

(i) Band-pass filter 0.1; disturbance, 59.5 ft/sec horizontal-velocity sharp-edge gust initiated at time 55 seconds.

Figure 9.- Concluded.

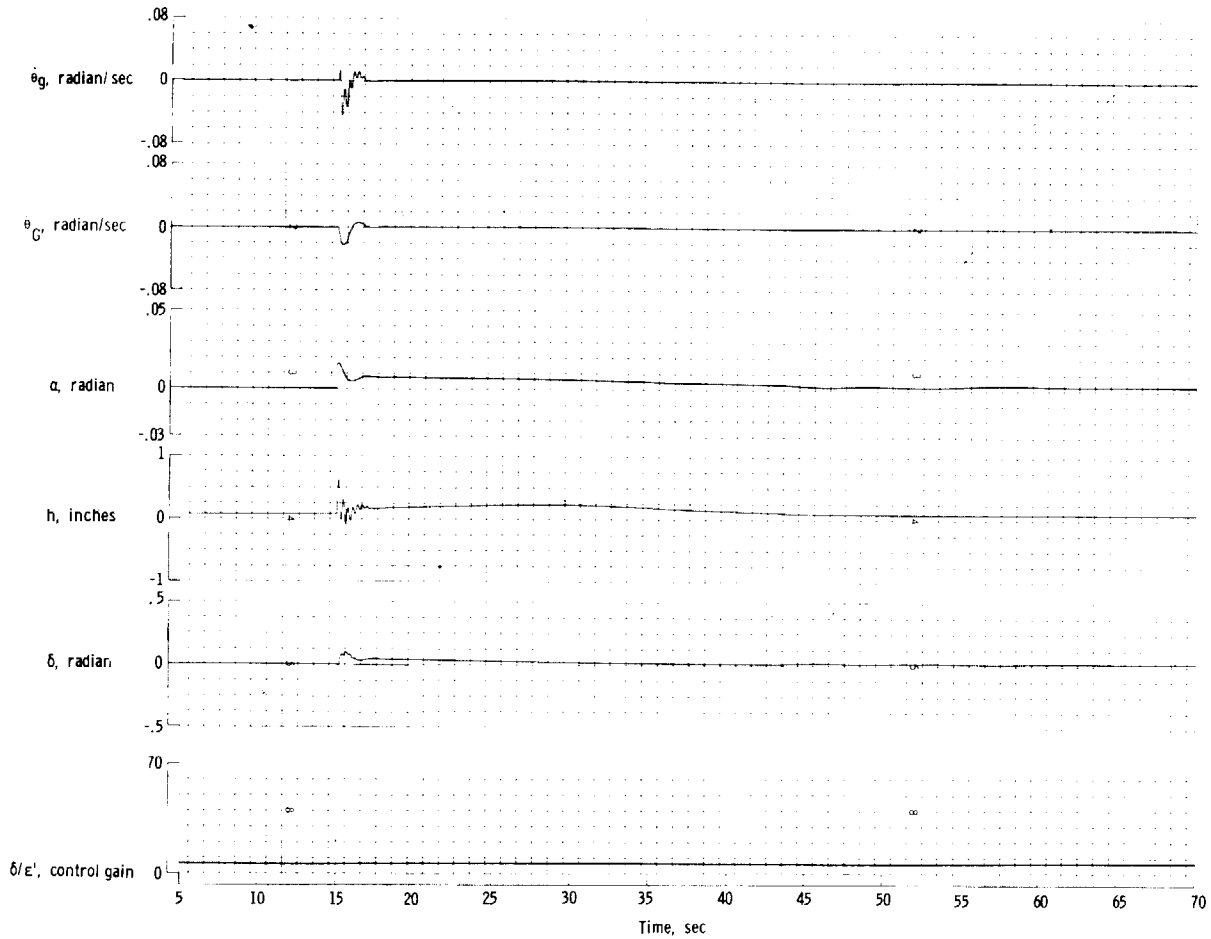

(a) Control gain 5; disturbance, sharp-edge gust of 21 ft/sec horizontal velocity initiated at time 15 seconds; sensor at station 646.

Figure 10.- Fixed gain (δ/ϵ') pitch-rate missile-control-system performance, trajectory portion from 5 seconds after launch to second-stage ignition.

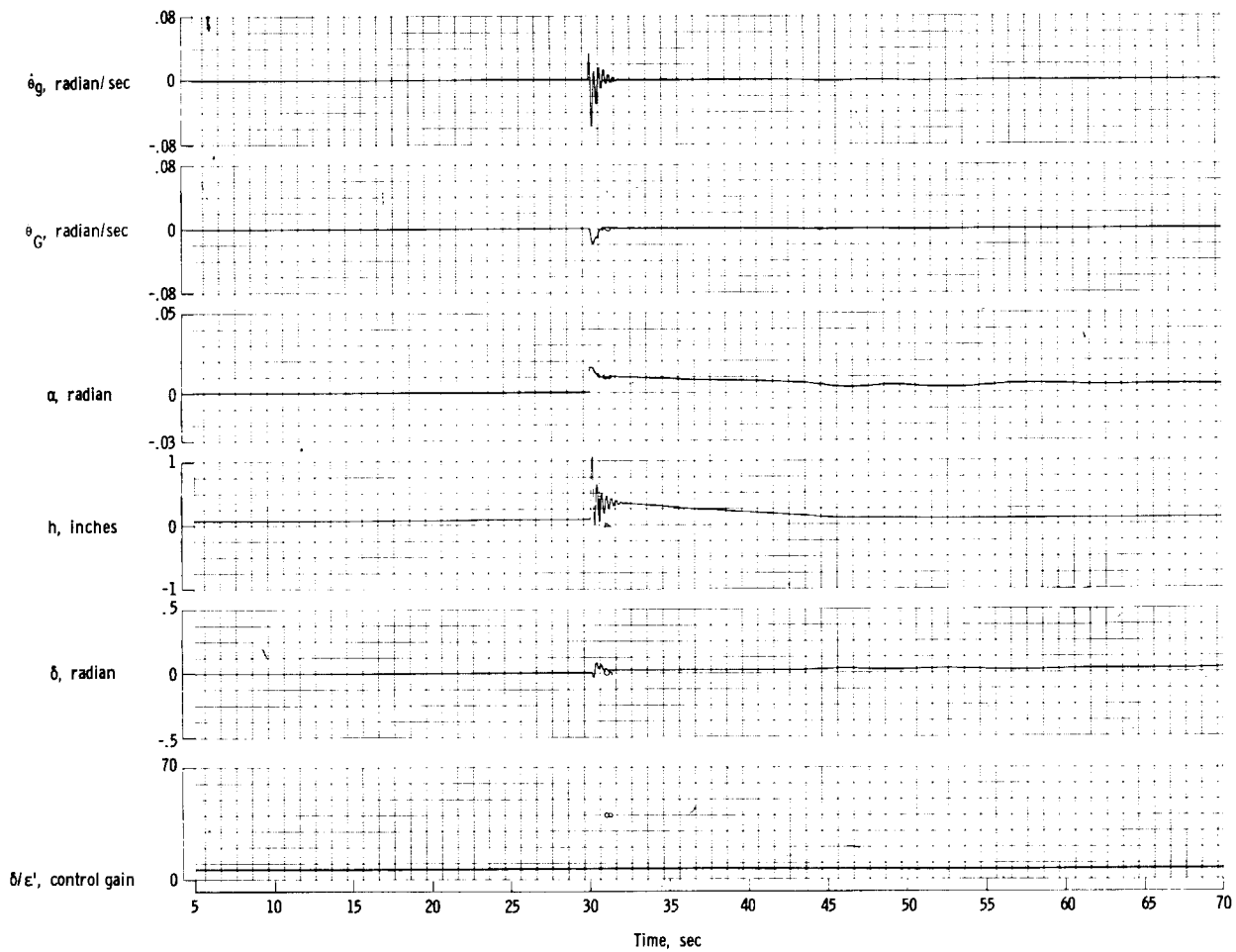

(b) Control gain 5; disturbance, sharp-edge gust of 57 ft/sec horizontal velocity initiated at time 30 seconds; sensor located at station 646.

Figure 10.- Continued.

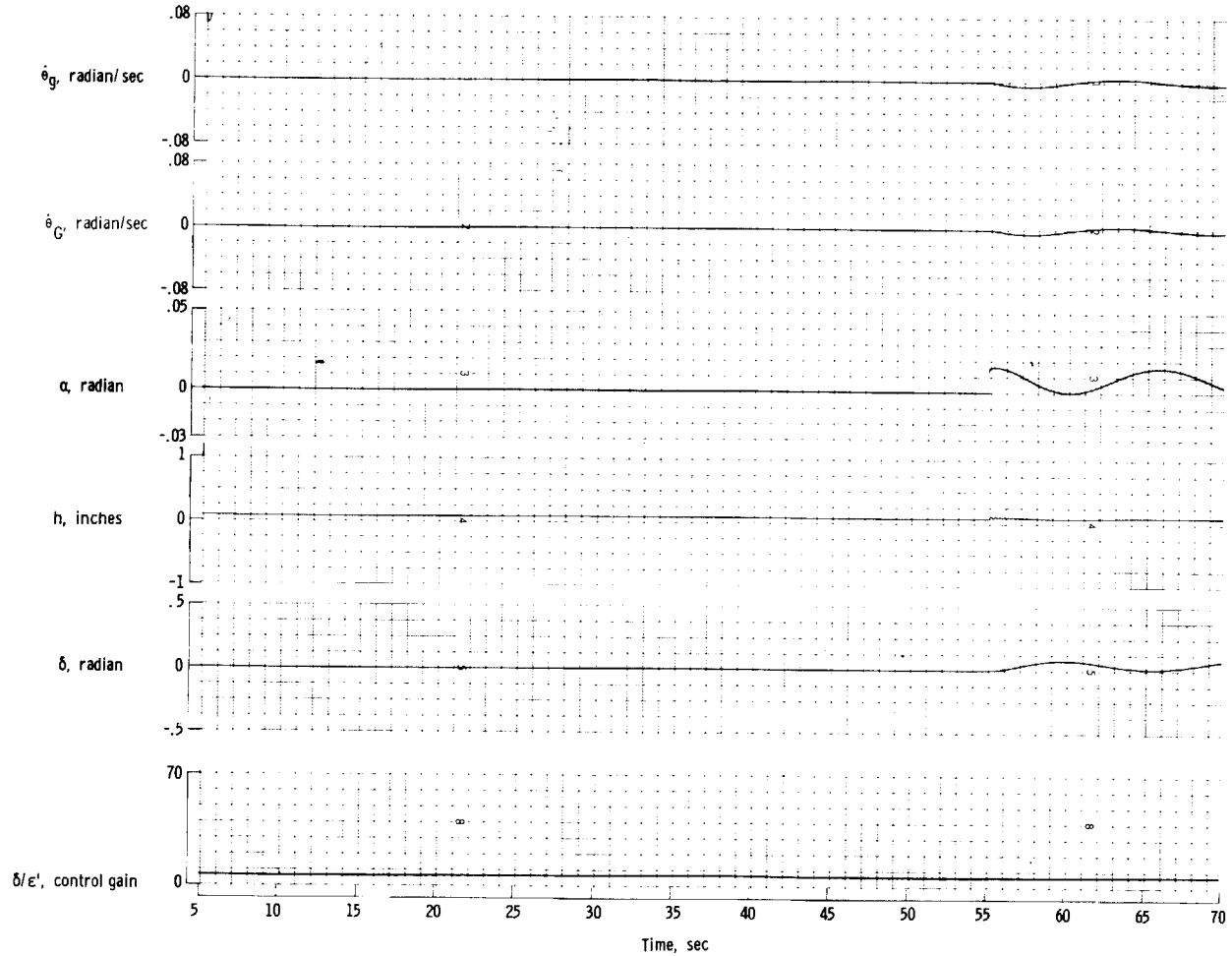

(c) Control gain 5; disturbance, sharp-edge gust of 59.5 ft/sec horizontal velocity initiated at time 55 seconds; sensor located at station 646.

Figure 10.- Concluded.

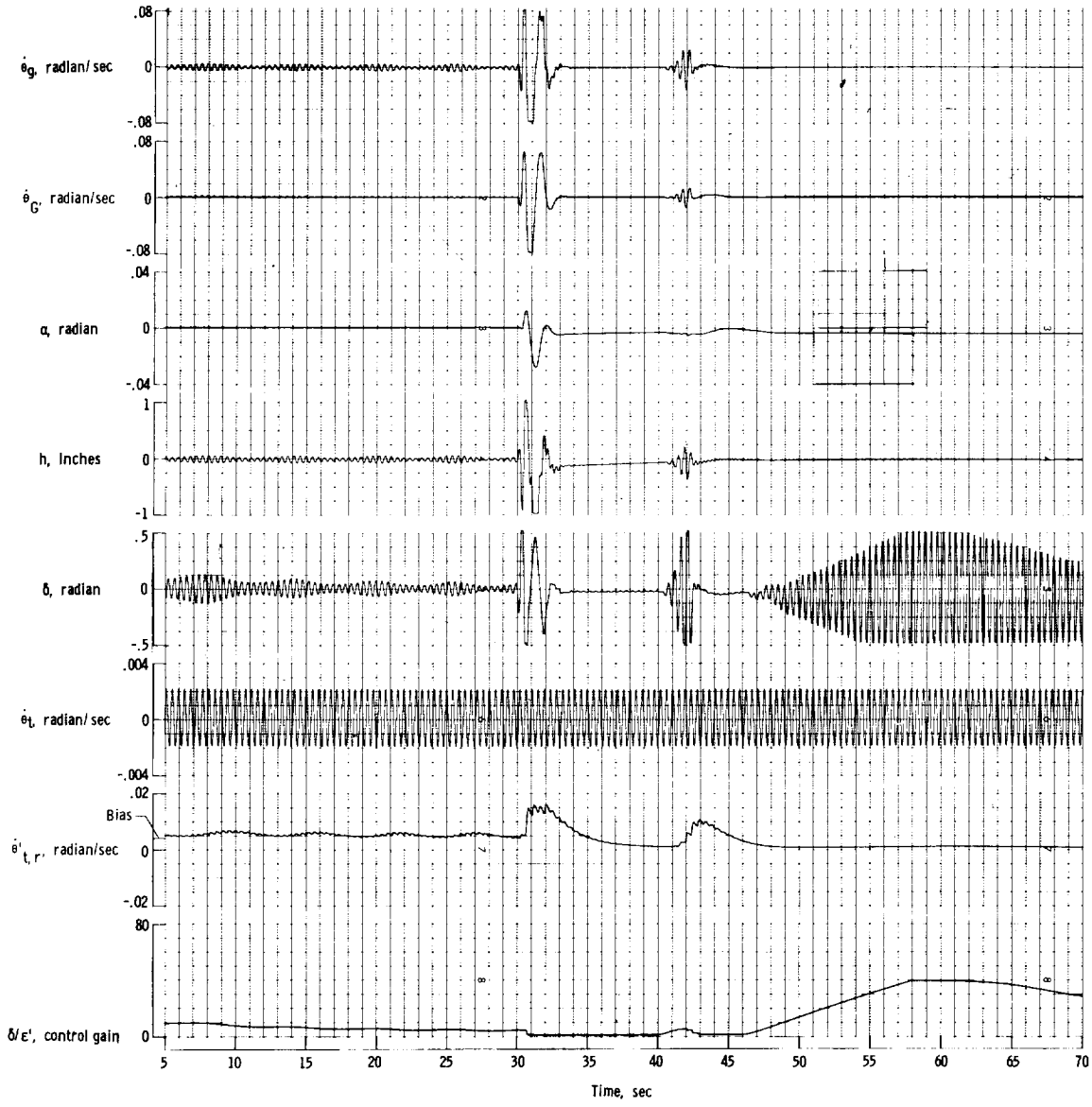

Figure 11.- Trajectory time histories demonstrating system ability to prevent control-induced instability; gain instability instantaneously introduced at time 30 seconds; sensor located at station 646.

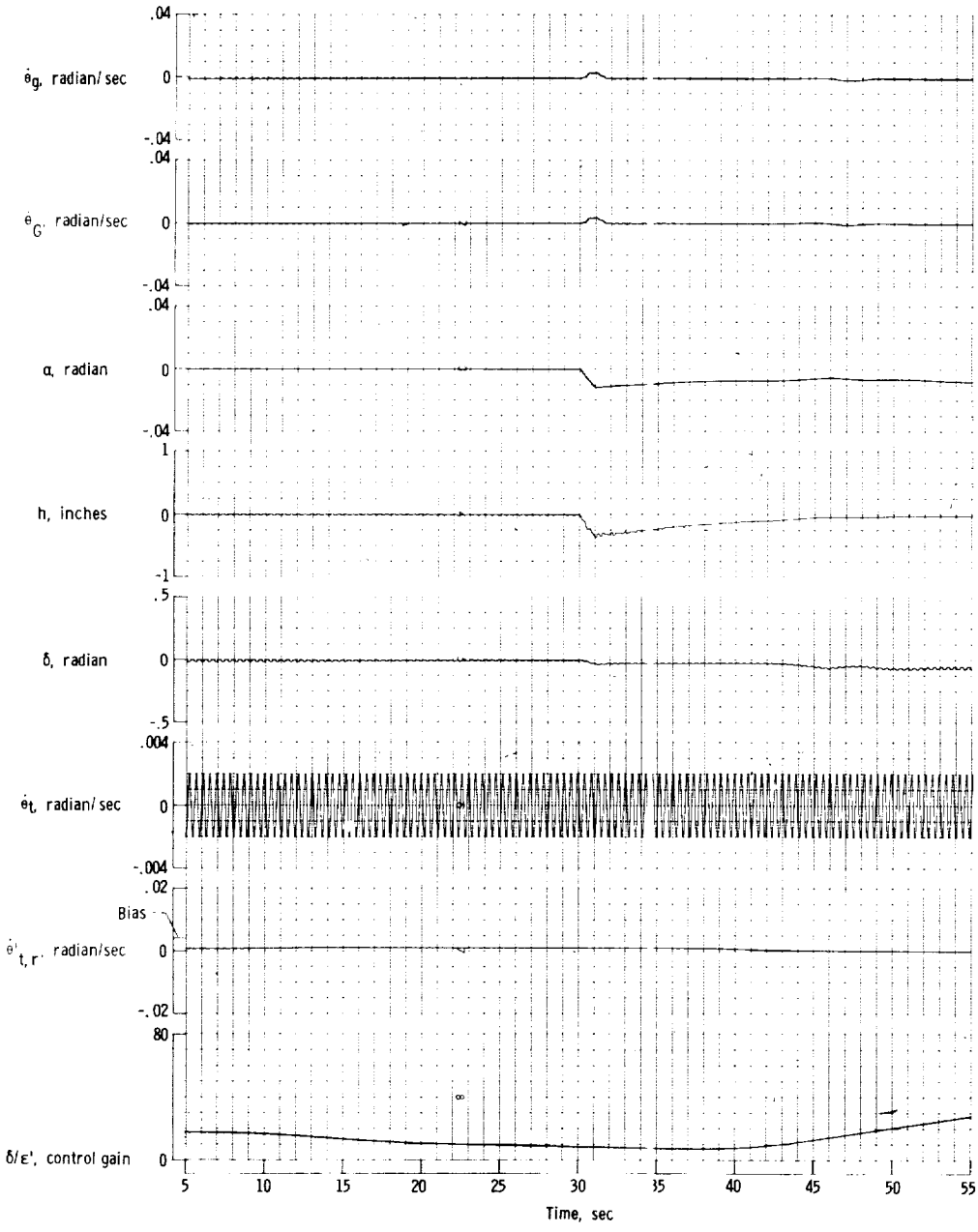

(a) Filter 0.05; sensor at station 400 λ_j = 0.000; disturbance, wind gust increasing from 0 to 21 ft/sec horizontal velocity in 1 second initiated at time 30.

Figure 12.- Trajectory time histories showing the effect of sensor location on adaptive pitch-rate missile-control-system performance.

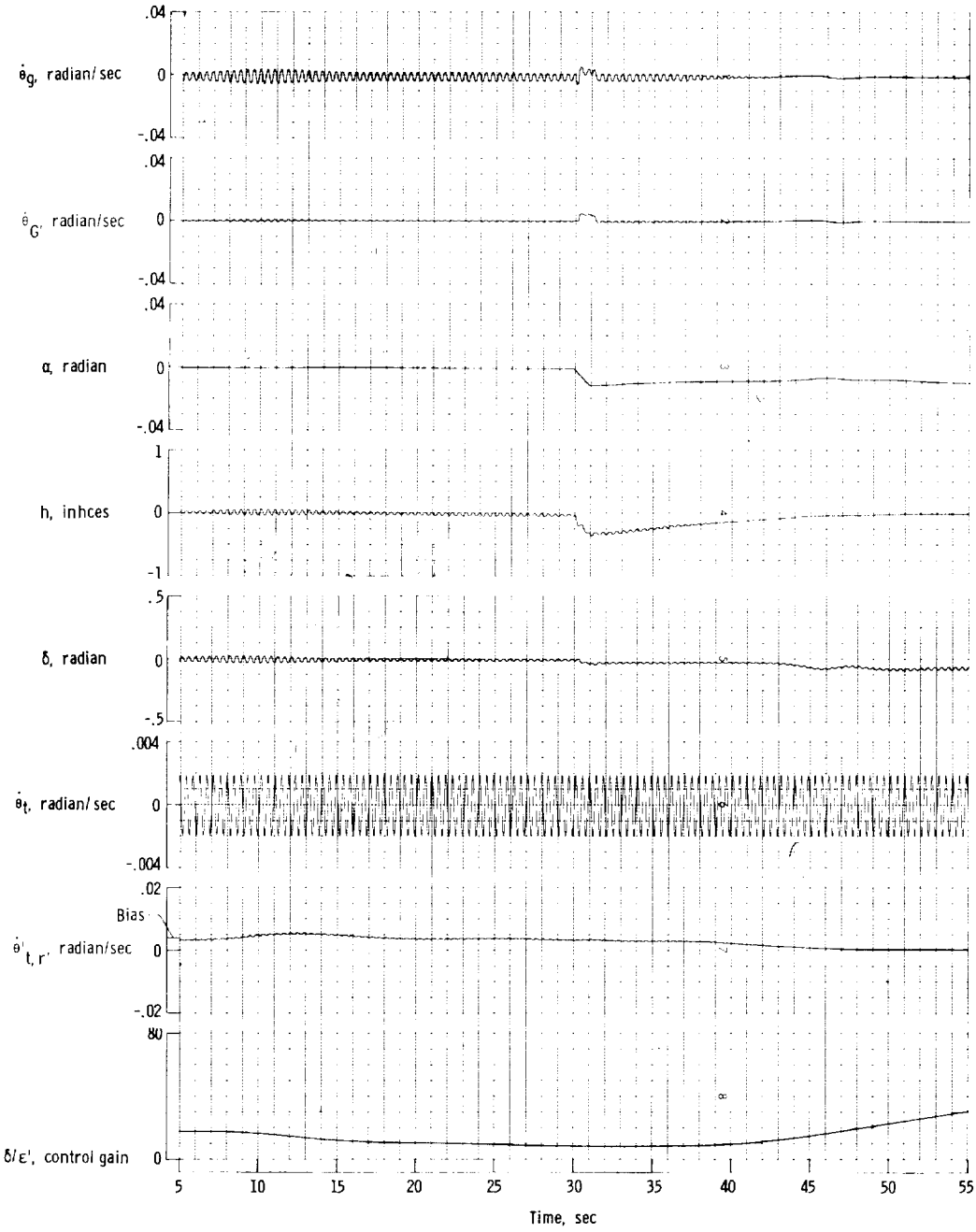

(b) Filter 0.05; sensor at station 646 λ_j = 0.0037; disturbance, wind gust increasing from 0 to 21 ft/sec horizontal velocity in 1 second initiated at time 30 seconds.

Figure 12.- Continued.

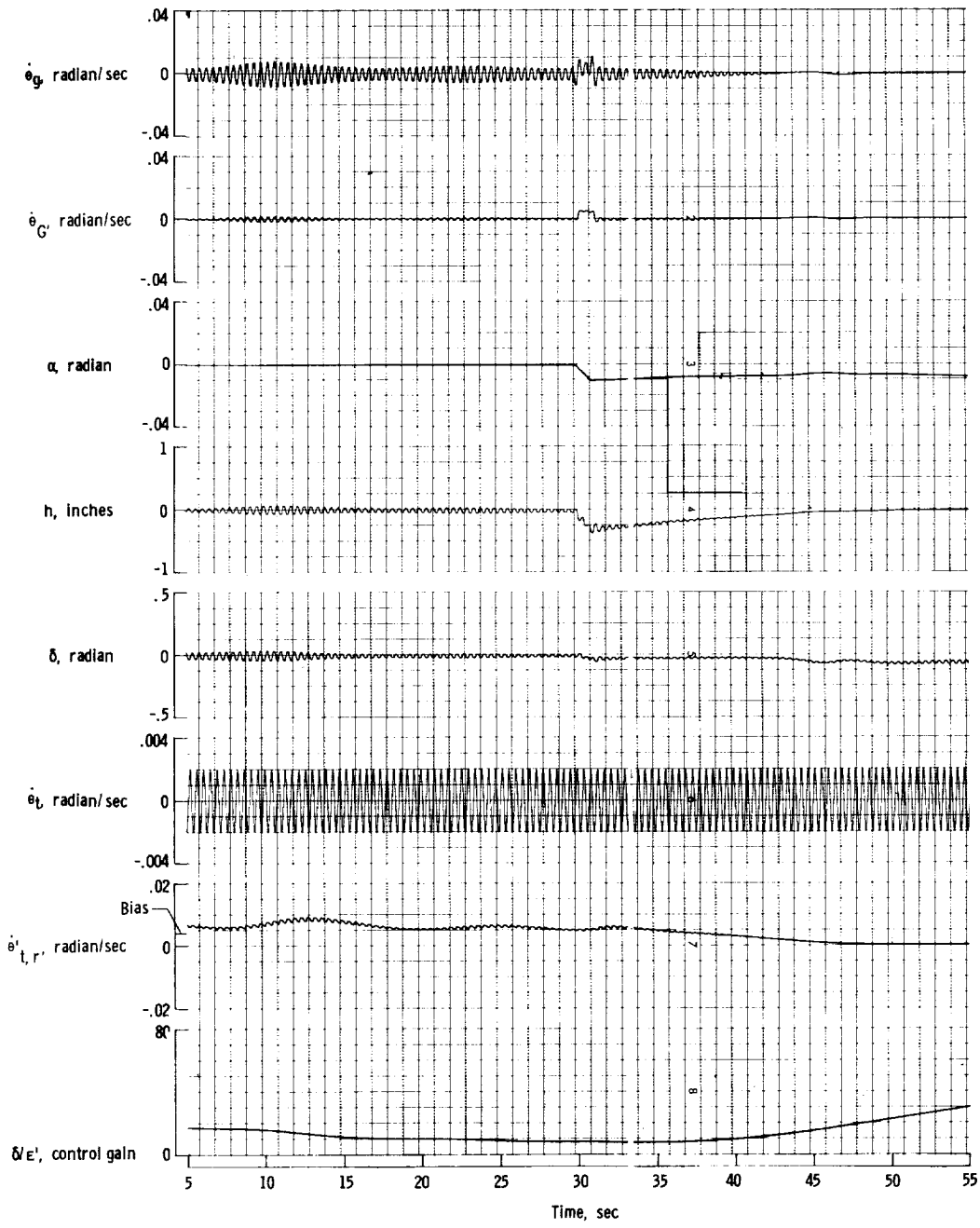

(c) Filter 0.05; sensor at station 746 λ_j = 0.0048; disturbance, wind gust increasing from 0 to 21 ft/sec horizontal velocity in 1 second initiated at time 30 seconds.

Figure 12.- Concluded.

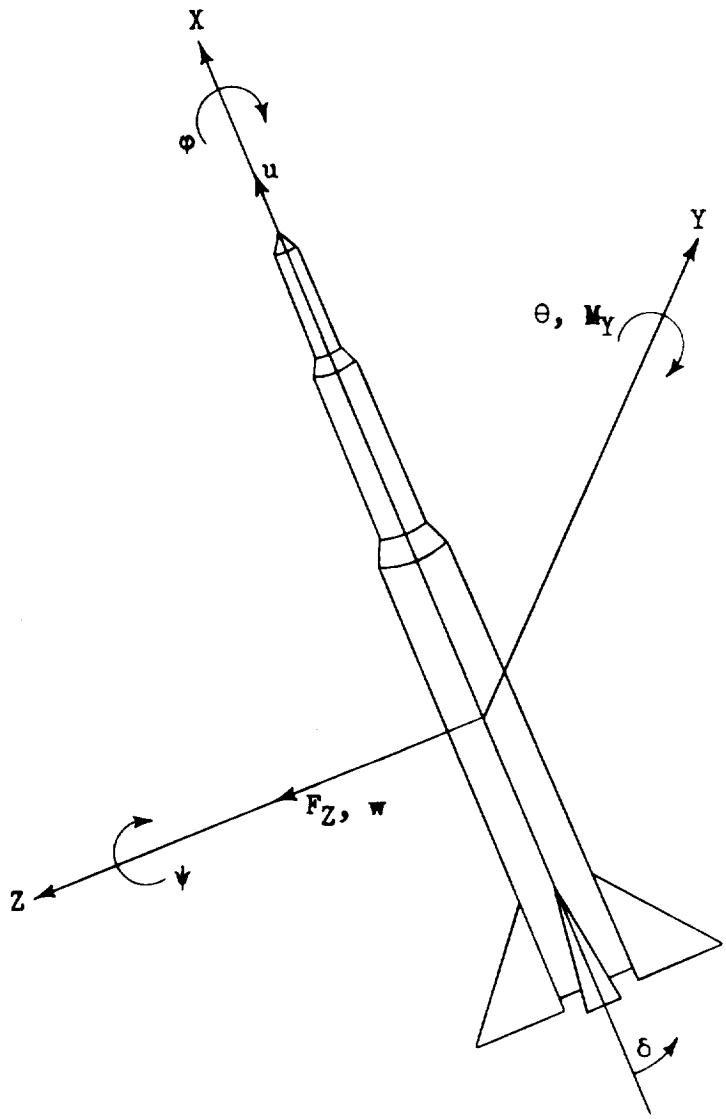

Figure 13.- Body-axes system employed with positive direction of forces, moments, and displacements shown.

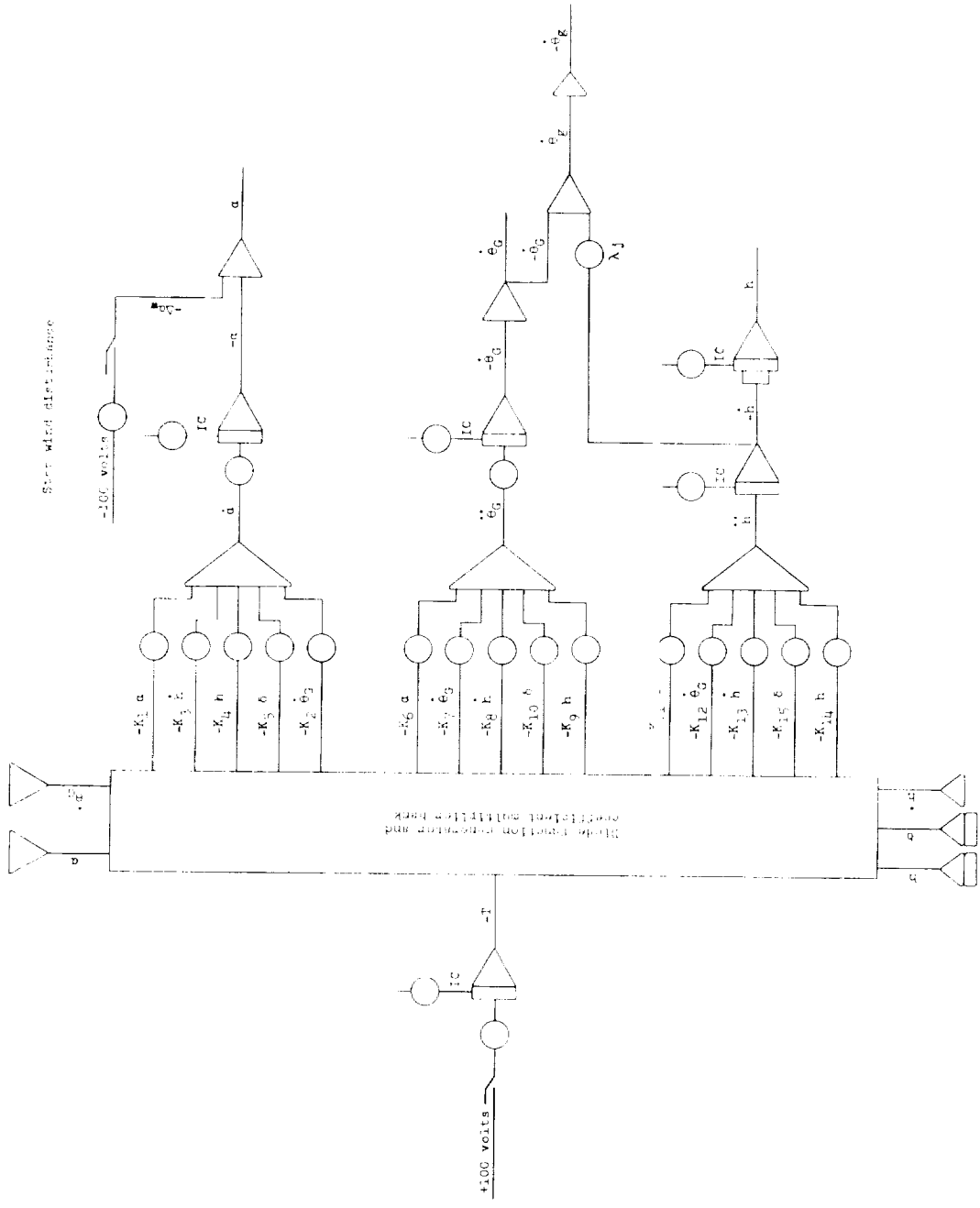

Figure 14.- Analog mechanization of equations of motion.

L-14956

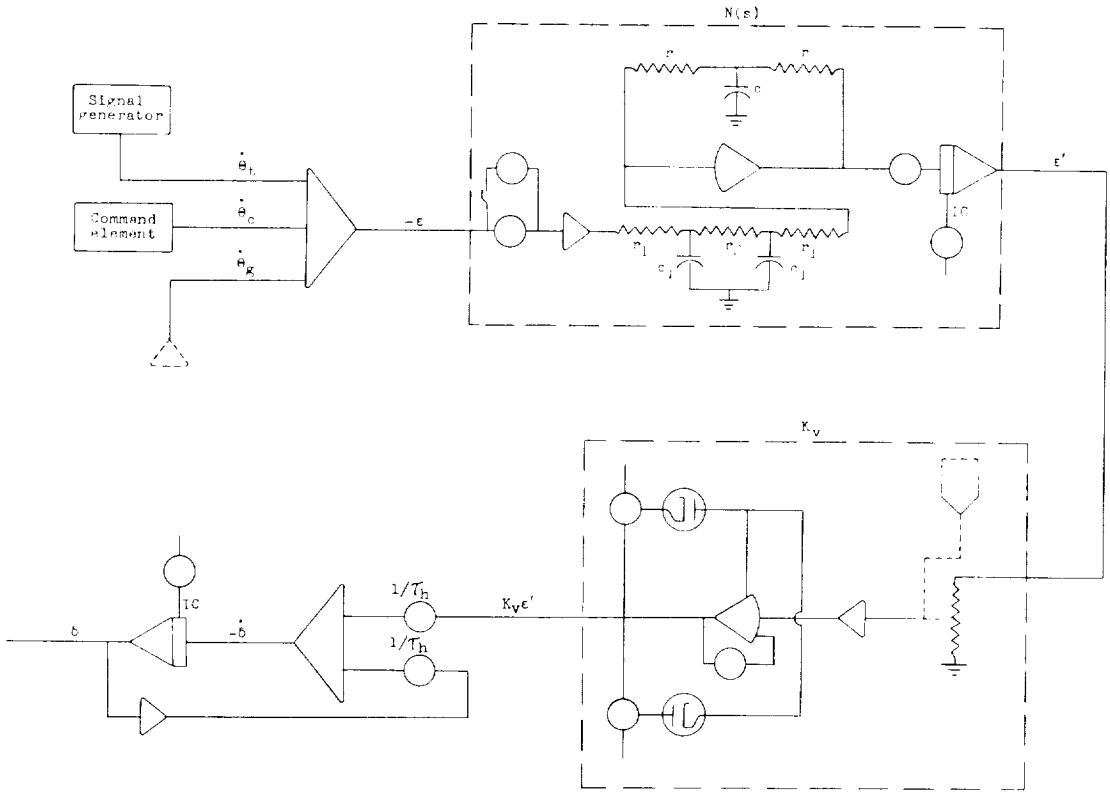

Figure 15.- Analog mechanization of forward-loop components.

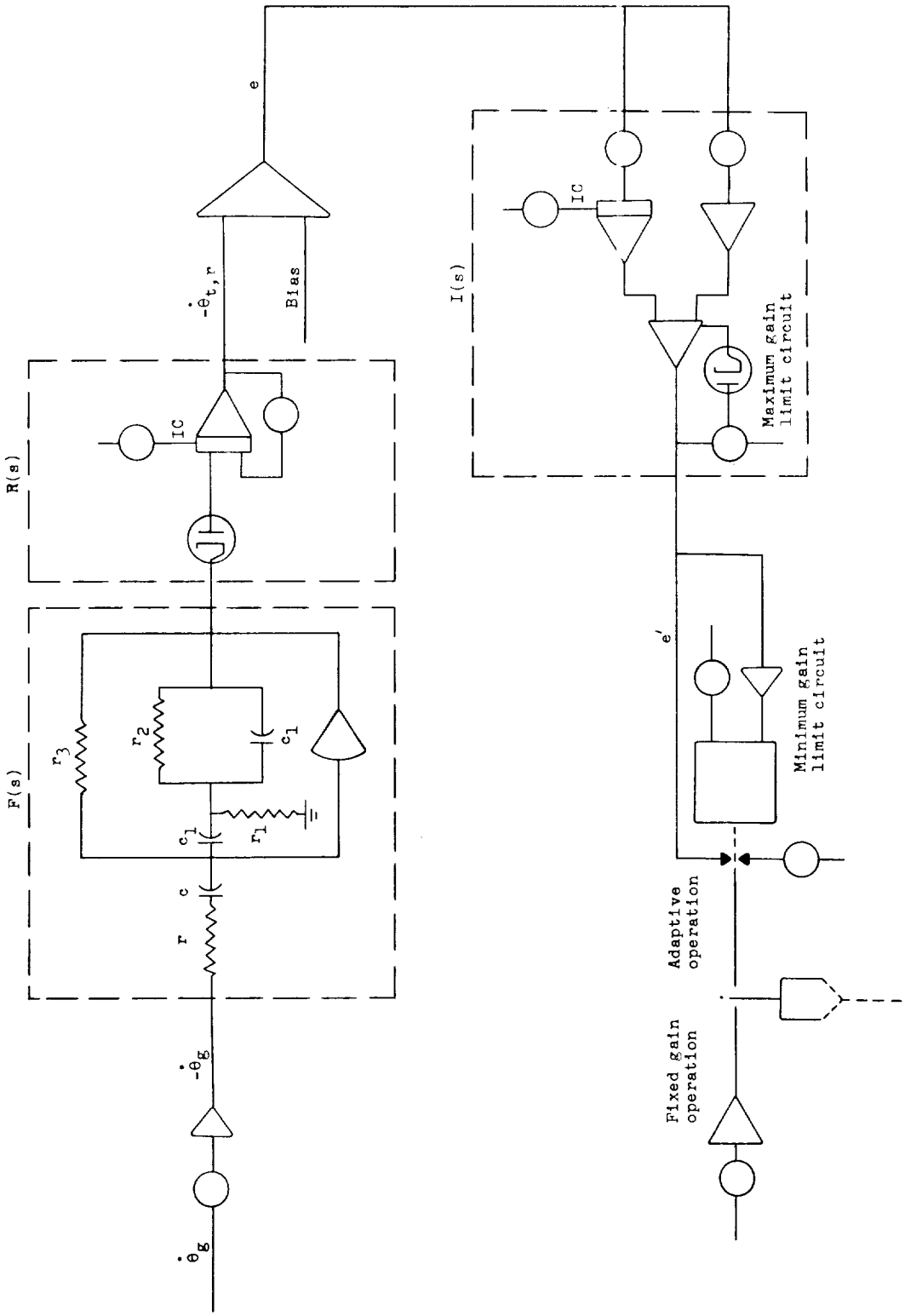

Figure 16.- Analog mechanization of adaptive-loop components.

L-1456